FOURTEENTH EUROPEAN ROTORCRAFT FORUM

Paper No. 8

AN EXPERIMENTAL INVESTIGATION OF THE DOWNWASH BENEATH A LIFTING ROTOR AND LOW ADVANCE RATIOS

I.C. CHEESEMAN AND C. HADDOW

DEPARTMENT OF AERONAUTICS AND ASTRONAUTICS
UNIVERSITY OF SOUTHAMPTON
SOUTHAMPTON SO9 5NH, ENGLAND

20 - 23 September, 1988
MILANO, ITALY

ASSOCIAZIONE INDUSTRIE AEROSPAZIALI
ASSOCIAZIONE ITALIANA DI AERONAUTICA ED ASTRONAUTICA

AN EXPERIMENTAL INVESTIGATION OF THE DOWNWASH BENEATH A LIFTING ROTOR AND LOW ADVANCE RATIOS

I.C. Cheeseman* and C. Haddow**

Department of Aeronautics and Astronautics
University of Southampton
Southampton SO9 5NH, England

ABSTRACT

An investigation of the downwash just beneath a lifting rotor has been made using triaxial hot wire probes. The rotor was operated at two low advance ratios using both near full scale tip speed and reduced tip speed. Comparison of the two cases showed that the flow was sensitive to tip speed in particular areas.

Careful checks were made to ensure that only results within the calibrated hot wire regions were accepted. Rev by rev data was taken.

1.0 INTRODUCTION

While many investigations of the induced velocity beneath a lifting helicopter rotor have been made little work has been done in forward flight. This paper reports the results of experimental measurements made, using triaxial hot wire anemometers, under a helicopter rotor in steady flight at low advance ratios ($\mu \leq 0.1$). This test programme was carried out using the University of Southampton High Speed Rotor (H.S.R.) rig mounted in the University 3.35 x 2.44m wind tunnel (Fig. 1). In addition measurements of the following parameters were made; blade bending moments, overall rotor pitching and rolling moments, lateral and logitudinal forces, thrust and torque. The investigation of the wake was limited to one plane beneath the rotor ($z/R = -0.075$).

2.0 THE ROTOR RIG AND DATA ACQUISITION SYSTEM

2.1 The Rotor Rig

The University of Southampton High Speed Rotor rig is a non-articulated model rotor of 1.35m diameter which has been designed to allow tests to be carried out at a tip Mach number comparable with those of full scale helicopter rotors. With this in view the maximum rotational speed is 4000 r.p.m., although typical measurements were made at 2500 r.p.m. corresponding to a tip Mach number of about 0.52. Drive is supplied to the rotor via a belt drive from a thyristor controlled variable speed 35 H.P. electric motor. The rotor can be utilised in either two or four bladed configurations.

Collective and cyclic settings on the H.S.R. were initially remotely controlled via electric stepper motors. At the thrust levels used for the test programme described here

---

* I.C Cheeseman is now Part Time Professor in the University of Southampton and Director (Research) with Stewart Hughes Ltd., Southampton.

** Dr. C. Haddow is now an Engineer-Programmer with Logica Space and Defence Systems.

this arrangement proved unsatisfactory. This was overcome by replacing the remote control system with a manual one with mechanical locking.

Due to the high centrifugal loads experienced by the blades the spars are constructed of carbon fibre with the surrounding blade profile moulded from polyurethane. A summary of the rotor characteristics is given in Table [1].

TABLE 1:

Rotor Type, Model, feathering	hinge		
Rotor Design			
No of Blades	2 or 4	Rotor Solidity (b = 4)	0.1132
Rotor Radius	0.675m	Blade Taper Ratio	1.0
Blade Chord	0.06m	Blade Twist	0°
Root Cut Out	0.281R	Aerofoil Section	NACA 0015
(ΩR)	0-280m/s		

Included in the rotor head assembly is a five component strain gauge balance. This enables measurement of thrust, side and H-forces, pitch and rolling moments. In order to enable accurate measurements of thrust to be made the shaft in the head assembly is connected to the drive shaft by means of a "zero thrust" coupling The upper shaft is also strain gauged to attempt measurement of torque.

2.2 Dynamic Balancing and Tracking

Dynamic balancing of the rotor was achieved using data from the force balances.

Trial weights of 5-10 gm were attached to a known blade. Using this data it was possible to calculate the magnitude and position of the weight required to mass-balance the rotor.

Blade tracking was carried out by mounting a T.V. camera looking at the rotor edge on. The blades were then illuminated by a high power strobe. From the resulting T.V. pictures it was possible to determine if any blade(s) were flying high or low (each blade being a different colour) and then the rotor was stopped and the pitch linkage on the offending blade(s) adjusted. This procedure was repeated until all blades were flying in the same plane.

2.3 Rig Instrumentation

2.3.1 Blade Instrumentation

On the "master blade" instrumentation consisted of twelve strain gauges mounted on the carbon fibre spar. These gauges were arranged in pairs to measure the blade flapwise bending moment. This system is by no means ideal since the energising voltages for the strain gauges as well as the output signals are prone to noise pickup from the slip rings. This problem was partially overcome by frequent cleaning of the slip-ring

unit, but even then sizeable noise signals were encountered. In view of this only ensemble averaged data was used in the subsequent analysis.

Calibration of the blade instrumentation was carried out by hanging a mass on the tip of the blade and monitoring the resulting output from the strain gauges amplifiers. Since the distances of the applied load from the strain gauge pairs were known it was possible to calculate the applied moment and, hence, a graph of voltage against moment could be plotted. A typical set of calibration curves obtained from the master blade is shown in Fig [2].

2.3.2 Rotor Balance

A schematic diagram of the rotor balance is shown in Fig [3]. The balance consists of eight strain gauged flexures, four (A-D) mounted vertically and the other four (W-Z) mounted horizontally. Lateral side force measurements were obtained from flexures A & C and longitudinal forces from B & D. Similarly, pitch and roll data were obtained from flexures X & Z and flexures W & Y respectively. Thrust was measured by using all four flexures W-Z. Since measurement of thrust and moments required that the strain gauges on flexures W-Z be connected to the amplifiers differently it was not possible to measure these simultaneously and a switch was used to select the required configuration.

Initial tests revealed that quasi-statically the above system worked well. Under dynamic conditions it was, only possible to obtain satisfactory thrust measurements. Measurements of apparently extremely large periodic forces and moments were obtained for the other four components. Modelling the system showed that filtering out the AC components gave acceptable mean values of all components.

All channels were calibrated by applying the appropriate static force or moment to the rotor hub. Since the balance is some way below the rotor a pure side force at the rotor results in the production of a moment as well as a side force at the balance. Both measurements were made and this information used to resolve moments and inplane forces from balances force and moment measurements. All calibrations were repeatable and linear.

Measurement of torque was attempted by fixing four strain gauge rosettes to the top end of the upper shaft. The low strain levels measured exaggerated the slip ring noise. A capacitor was again used to provide a low-pass filter. The torque figures quoted were obtained by averaging all values obtained under the same conditions.

2.4 Determination of Blade Flapping

The blade flapping was determined from the measured bending moments by the method of assumed modes. The blade modes used in the analysis were calculated using a program developed by Azzam.

Due to the strain gauge fatigue problems 3 gauge pairs were available for the first test condition only. Since the 3rd mode amplitude is typically an order of magnitude less than that of the first mode, this estimate is considered acceptable.

For the other test conditions only 1 guage pair was available. The flapping angle calculated for the first test condition for both 1 and 3 modes (1 and 3 guage pairs respectively) is shown in Fig. [4]. The main difference is in the higher hamonic components of the flapping.

2.5 Data Acquisition System

The data acquisition system used in this project consisted of a DEC LSI 11-23 computer fitted with two Intercol Systems sixteen channel analogue to digital scanner

units. User interface to the system was via a Tectronix 4006 V.D.U. or a Decwriter LA34 terminal.

The software controlling data acquisition provided selection of the input channels scanned, the data acquisition rate and the number of samples taken. With the scanners operating in interleaving mode the maximum available data acquisition rate was 50000 samples per second. Typically on tests carried out on the H.S.R. rig ten channels of data were recorded giving a maximum scanning frequency per channel of 5kHz, or a resolution of 3° of azimuth at 2500 r.p.m.

3.0 THE VELOCITY MEASURING TECHNIQUE

3.1 Introduction

To investigate the induced flow field of a helicopter rotor in forward flight the first difficulty to be overcome is the development of a system capable of measuring accurately in the highly three-dimensional flow.

The technique used was a tri-axial constant temperature hot-wire probe coupled with a PDP 11-23 mini-computer which provided data verification and analysis. When out of range the computer alerted the operator who could then make the necessary adjustment.

3.2 Measuring Principle

The basic pinciples of hot-wire anemometry are widely understood, and will not be repeated here.

L.V. King in 1914 developed a theory for the heat loss from a hot-wire in incompressible flow.

Various authors, have modified his work resulting in the commonly used Kings law.

$$V^2 = A + B\,U^n \qquad [1]$$

where V is the Wheatstone Bridge voltage, U the fluid velocity and A, B and n constants, n typically having a value of about 0.45.

Equation [1] assumes that the flow passing the hot-wire is orthognal to the wire and parallel to the supports holding the wire. If this is not the case, it is necessary to replace it by the effective cooling velocity U_{EFF}. Jorgensen (Ref [1]) and others have suggested the use of Equation [2] to define U_{EFF}.

$$U_{EFF}^2 = k_1{}^2 U_x^2 + U_y^2 + k_2^2 U_z^2 \qquad [2]$$

k_1 and k_2 are the directional constants of the wire. Fig. [11] shows the velocity components relative to the sensor.

Ideally constants k_1 and k_2 would be determined individually for each separate wire. This is an extremely time consuming procedure involving making measurements at a considerable number of yaw and pitch settings for each wire. It was not possible to carry

out the required measurements for each wire and so the values of k_1 and k_2 = 1.02 used were based on work by Jorgensen.

The type of probes used throughout these investigations were DISA type 55P91. This probe consists of three separate wires mounted so as to be mutually orthognal. Each wire is 3.4mm in length with an active region of 1.25mm and has a diameter of 5 μm leading to an L/D of 250. The wires are arranged in a symmetrical manner about the probe body-axis, each inclined at an angle of 54.8° to this axis and the active portions of all the wires lie in a sphere of 3 mm in diameter.

Due to the geometry and construction of the probe a flow velocity vector must lie within a cone having an apex angle of 35.2° with respect to the probe body axis if it is to be uniquely defined. This has obvious implications for the usefulness of tri-axial hot-wire probes in flow regimes where very large variations in direction occur and these are discussed later.

3.3 Calibration

Conventional calibration techniques for tri-axial hot-wire probes involve the determination of five constants for each wire, A, B, n, k_1 and k_2. Huffman (Ref [2]), for instance, has developed a technique which employs the use of two data sets for each wire, one at variable velocity and fixed angle, the second at fixed velocity and variable angle. Since the calibration process was extremely time consuming it was necessary to devise a quicker method.

This used fixed directional coefficients as previously described and calibrated all three wire's simultaneously. This was achieved by orientating the probe body-axis at a known angle to the flow (typically parallel to the flow) and measuring the output from the bridges at a variety of tunnel speeds in the range 0-40 m/s.

Data from the hot-wires was averaged over one minute at each speed. Ambient temperature and pressure, Betz gauge reading and probe orientation. At zero flow velocity due to the close proximity of the sensors to each other, the heating of the surrounding air caused errors in the output from the wires. This was overcome by making the zero flow measurements on each wire individually, i.e. with one wire ACTIVE and the others on STANDBY.

The effective cooling velocity was determined from the Betz gauge reading corrected for ambient temperature and pressure.

With the effective cooling velocity at each wire known for a variety of tunnel velocities a least squares search algorithm was used to determine A_i, B_i and n_i (i = 1, 3) by minimising;

$$Q_i = \sum_j \left(A_i + B_i U_j^{n_i} - E_{ij}^2 \right)^2 \qquad [j = sample\ number] \qquad [3]$$

3.4 Data Analysis

Three traps were used to detect cases when the velocity was outside the 35.2° cone of acceptance. These were (a) when the voltage output drops below the calibration zero voltage, (b) components of the effective velocity matrix can become complex and finally (c)by calculating the angle between the measured flow vector and the probe body-axis and deleting cases where the angle is > 25°.

3.5 Error Estimates

To determine the accuracy of the hot-wire probe, it was mounted in a wind tunnel parallel to the tunnel centre line and calibrated as previously described. After calibration a set of measurements were made at a constant tunnel speed but with different probe orientations.

The differences between the actual flow and the measured flow were then calculated. The error in the magnitude for all probe angles $< 20°$ is $\leq 2\%$. Also, the error in determination of the flow direction is $\leq 2°$ in both pitch and yaw for flow inclinations $< 15°$. Outside of this the error increases to $\sim 3.5°$ at inclinations of $25°$.

These errors are not solely due to the probe, but also include those due to uncertainties in the probe orientation, particularly in the yaw setting.

4.0 TEST CONDITIONS

The lower limit to the advance ratio that could be studied was influenced by two factors. One was recirculation problems in the tunnel, the other was the acceptance cone of the hot-wire probe. This limit was found to be about $\mu = 0.067$ and even here, at some locations, it was not possible to obtain acceptable data. The highest advance ratio studied was $\mu = 0.1$. All tests were made at a disc loading approximately equal to that of the Westland Lynx. The actual value was limited by the onset of stall flutter of one of the blades on the retreating side. The velocity measurements clearly show differences between this "rogue" blade and the other three and this is discussed later.

Rotor speed was either 2500 r.p.m. or 1250 r.p.m. the former giving a tip speed only slightly below that of current helicopters. All measurements were carried out with the rotor approximately trimmed in roll and with a forward inclination typical of the Lynx at the advance ratio.

Table [2] summarises the flight conditions for which measurements were made;

TABLE 2: Test Conditions

Cond	Coll	A1	B1	R.P.M.	μ	Ct	Cq
1	7.5°	0.75°	0.25°	2500	0.1	0.0062	.00040
2	7.5°	0.75°	0.25°	2500	0.067	0.0052	.00044
3	7.5°	0.75°	0.25°	1250	0.067	0.0055	.00045

Tunnel calibration showed that at the position of the rotor in the tunnel the flow is inclined downward at $1.75° \pm 0.25°$ at the speeds at which the tests were made. Thus, the rotor was effectively tilted forward by this amount.

The rotor was trimmed in roll by adjusting the cyclic pitch until the bending moment at the root of the master blade (as measured by the blade strain gauges) was the same at 90° and 270° azimuth.

Within the accuracy of the measurements it was found that the same cyclic settings were suitable for trimming at both μ = 0.1 and μ = 0.067 and these are as shown in Table [2].

Validation of the above trimming method can be seen in Fig. [5] which show the time averaged vertical velocity data w.r.t. azimuth. The symmetrical distribution of the rotor downwash (Z-compt) about the longitudinal axis, indicates satisfactory roll trim.

An important objective of these experiments was to try to determine the flow field at the rotor blades. The vertical position of the probe was chosen to be as close to the rotor disc as possible, namely z/R = -0.075, or approximately 5cm below the stationary rotor.

The normal azimuth increment between measuring stations was 30°, although at positions where interesting flow details were noted this was reduced. Radial measuring positions were mainly concentrated in the outer region of the blade. No data was collected inboard of 0.6R since it was found that the hub caused considerable turbulence and, hence, orientation problems for the hot-wire further inboard. Measurements were made outboard of the tip at up to 1.2R where definite evidence of close tip vortex passages were observed. Table [3] summarises the positions used for wake measurements.

Two coordinate systems are used for presenting the velocity data. The first is centred on the hub. With Z positive vertically upwards w.r.t. the hub, Y positive to port and X positive upstream.

The second axis system is fixed in the blade and is related to the non rotating coordinates by:

$$\left[V_{SPANWISE}\ ,\ V_{CHORDWISE}\ ,\ V_{VERTICAL}\right] = \begin{bmatrix} -\cos\Psi & -\sin\Psi & 0 \\ \sin\Psi & -\cos\Psi & 0 \\ 0 & 0 & 1 \end{bmatrix} \begin{bmatrix} V_X \\ V_Y \\ V_Z \end{bmatrix} \quad [4]$$

- note the rotation is clockwise viewed from above the rotor.

This second axis system is useful in examination of the blade bound circulation and the tip vortex, since they are approximately parallel to these axes as the blade passes over the probe.

5.0 TIME AVERAGED VELOCITY DATA

5.1 Scaling at constant μ - varying tip speed

An important measure of the induced velocity is the average time history for one rotor revolution at each probe position. The signals were therefore time averaged over up to 35 consecutive revolutions when conditions permitted.

Typical time averaged non-dimensionalised velocity plots are shown in Figs. [6 & 7] for μ = 0.067 at the two tip speeds listed. Inspection reveals there is, a considerable degree of agreement between both data sets.

Differences exist first in the Z-component at 0.6R between Ψ ~90°-270° where there is a difference of 15%-20%, with the data from 2500 r.p.m. giving the highest downwash values. This region is one where, at low advance ratios, the flow is heavily influenced by the

TABLE 3: Wake Measurement Positions

(N.B. 1, 2, 3 refer to test conditions previously defined)

Azimuth	0.6	0.8	0.9	0.95	1.0	1.05	1.1	1.15	1.2
0	1 2 3	1 2 3	1 2 3	1 2 3	1 2 3		1 2 3	2 3	1
15			2 3	1 2 3	1 2 3	2 3	1 2 3	1	1
30	1 2 3	1 2 3	1 2 3	1 2 3	1 2 3		1 2 3	1	
60	1 2 3	1 2 3	1 2 3	1 2 3	1 2 3		1 2 3		
90	1 2 3	1 2 3	1 2 3	1 2 3	1 2 3		1 2 3		
120	1 2 3	1 2 3	1 2 3	1 2 3	1 2 3		1 2 3		
150	1 2 3	1 2 3	1 2 3	1 2 3	1 2 3		1 2 3		
180	1 2 3	1 2 3	1 2 3	1 2 3	1 2 3		1 2 3		
210	1 2 3	1 2 3	1 2 3	1 2 3	1 2 3		1 2 3		
240	1 2 3	1 2 3	1 2 3	1 2 3	1 2 3		1 2 3		
270	1 2 3	1 2 3	1 2 3	1 2 3	1 2 3		1 2 3		
300	1 2 3	1 2 3	1 2 3	1 2 3	1 2 3		1 2 3		
330	1 2 3	1 2 3	1 2 3	1 2 3	1 2 3	2 3	1 2 3	1	
345			2 3	1 2 3	1 2 3	2 3	1 2 3	1	1

tip vortices from the leading edge of the rotor disc. These have first been carried back above the blades and then passed down through the rotor disc. In view of this it seems likely that the difference is due in some measure to the way in which the blade/vortex interaction takes place. This may be due to differences in the vortex structure and/or strength or the blade flapping at the different tip speeds.

Second in the region Ψ = 270° - 360°. The peak Z component occurs at 0.95R for the 1250 r.p.m. case, as opposed to 0.9R for the 2500 r.p.m. case. There are also disparities in the X-component, where for the 1250 r.p.m. case, there is an increase at all radial stations at Ψ = 300°, particularly at 1.1R, over the 2500 r.p.m. results. The converse of this is true for the Y-component where for r/R>0.8 the 2500 r.p.m. velocity shows considerable enhancement over the 1250 r.p.m. case.

These discrepancies may be due to differences in the tip vortex structure or trajectory, since the fourth quadrant is where these vortices undergo the most involved interactions with each other.

The implication of the above is that results obtained at the same advance ratio, but different tip speeds do not directly scale. These results are discussed later.

5.2 Rotor Wake Roll-Up

The mean values of the velocity components show that the roll-up of the rotor wake starts to occur a very short distance behind the rotor and indeed is rapidly completed. For μ = 0.1 at measuring stations in the vicinity of Ψ = 60° and 300° the Y-component of the flow (Fig [5]) is outboard from the rotor, with the magnitude increasing out to ~1.0R, after which it falls off again. Also, the X-component of the flow in the region of 1.1R shows a marked increase. The implication is that the wake is beginning to roll up into "fixed wing" type trailing vortices with cores lying in the vicinity of 0.95R from the rotor longitudinal axis. This is in general agreement with Velkoff et al (Ref [3]), Heyson & Katzoff (Ref [4]) and Spreito & Sachs (Ref. [5]).

The results obtained at μ = 0.067 also demonstrate this effect. However the Y component is now inboard and of somewhat greater magnitude. This change in the Y-component suggests that the vertical position of the vortices has changed and are now below the probe.This change is not unexpected since the flow skew angle is greatest at lowest μ.

5.3. Comparison with Glauert Model

Simple induced velocity formulae obtain are valuable for overall rotor performance and control estimates. For the normal component of the induced velocity an expression often used is the empirically derived Glauert Formula (Ref [6]);

$$V_i = V_{io}\,(1 + K\, r \cos\Psi) \qquad [5]$$

$$Where\ V_{io} = T/2\ \rho\ A\ \sqrt{V^2 + V_{io}^2}$$

the symbols having the usual meaning.

Knowing thrust, forward speed and the normal parameters equation [5] is solved for the induced velocity V_{io}.

The value of K is often determined from the expression derived by Coleman et al (Ref [7]);

$$K = \tan(\chi/2) \qquad [6]$$

Where χ is the wake skew angle given by

$$\chi = tan^{-1}(\mu/\lambda), \mu = \frac{V\cos\alpha}{\omega R}, \lambda = \frac{V\sin\alpha - V_{io}}{\omega R}$$

and α is the rotor angle of attack.

To compare the values from Equation [5], which holds at the rotor disc, with the experimental data obtained from a plane 0.075R below, the following assumptions are made:

A. The centre of the wake moves away from the rotor with an angle equal to the skew angle.

B. The wake contracts uniformily.

In view of the lack of data about wake geometry in forward flight the data obtained by Langrebe (Ref [8]) for the hover case was used to determine the wake contraction at 0.075R below the rotor. The results obtained using the value of K from Equation [6] are shown for example in Fig [8]. The agreement is very poor.

Using the method of least squares to obtain a best fit value of K was obtained. Table [4] summarises the calculated and fitted values of K;

TABLE 4: Values of K

Test Cond	K = tan (χ/2)	K (fitted)	% Difference
1	0.74	1.07	45
2	0.61	0.96	57
3	0.59	0.92	56

The above suggests that the appropriate value of K to use in Equation [5] is some 50% higher than that calculated from Equation [6]. This is in agreement with the findings of Ref [9] where an analysis carried out after the crash of the A.B.C. demonstrator aircraft indicated that the K value used in determining control requirements was too low. In particular Ref [9] indicates that the appropriate value of K should have been ~50% greater than that calculated.

5.4 Frequency Content of Wake

The frequency content of the wake was determined using Fast Fourier Transforms (F.F.T.s) on the velocity time histories to obtain Power Spectral Density (P.S.D.). For the F.F.T.s the data from each measuring position was examined to find a continuous record of 1024 acceptable data points, which correspond to ~8½ rotor revolutions. Examination of the P.S.D.s reveal, not unexpectedly, that essentially all of the energy in the wake spectrum is concentrated in frequencies which are multiples of the rotor frequency. Further the

dominant components are predominantly multiples of the fourth harmonic, particularly the 4th, 8th and 12th e.g. (Fig. [9]).

Since the rotor under test was four bladed this is not surprising. What is interesting is that at certain positions there is an appreciable 1 per rev component e.g. Fig. [9] shows the results from $\mu = 0.1, \Psi = 270°$.

To investigate this 1/rev variation the Fourier Series of the Ensemble averaged data was obtained with respect to the chordwise and spanwise coordinate system previously discussed. The analysis was made as one blade (orange) was known to be behaving slightly differently to the other three. To remove any small random 1/rev variation weighting the data, the 1/rev peak was ignored if the power content in the first harmonic was <5% of the power of the 4th harmonic at a particular position.

Examination of the 1/rev phase angle with probe azimuth position is seen in Fig. [11] when the as expected slope of -1 was generally found. Phase was calculated w.r.t. the master blade (white) positioned at $\Psi = 0°$.

The spanwise velocity component in Fig [10] shows that the maximum value occurs ~30° before the master blade passes over a given measuring station. As the orange blade lags the master blade by 270° the maximum value due to the 1/rev spanwise variation thus occurs some 60° after the orange blade passes overhead. This implies that the trailing vortices from the blades, induce velocities in the outboard direction, and hence, the trailing vortex from this blade is slightly stronger or nearer to the probe than those of the others.

The above observation is supported by analysing the vertical 1/rev variation. This shows that the maximum 1/rev upwash occurs about 270° before the master blade passes overhead a given probe position, thus implying that the maximum upwash occurs round about the time the orange blade passes overhead. This is consistent with the orange blade having a greater circulation than the others.

The chordwise 1/rev velocity variation does not, provide good agreement with the above. Chordwise flow is taken as being positive in the direction opposite to rotation, i.e. in the direction opposite to that induced by the blade circulation as it passes overhead. Thus, one expects, a minimum in the chordwise 1/rev variation when the orange blade passes overhead. Instead the maximum value occurs about 30° in advance of the orange blade passage. It should be noted that the chordwise 1/rev velocity component is small and errors correspondingly greater.

Overall these results indicate that the cause of the observed 1/rev variation is due to small differences in lift performance of one blade, viz the orange blade.

6.0 DETERMINATON OF BLADE BOUND CIRCULATION, TIP VORTEX ROLL UP, STRENGTH AND POSITION

From the ensemble averaged velocity data it is possible to extract a considerable amount of information regarding the blade bound circulation and the tip vortex roll-up, strength and position. This work has, in the past, been carried out primarily for the hover case which in many respects presents a considerably simpler problem in that there is, ideally, no variation with azimuth. Langrebe (Ref [8]) has carried out extensive measurements for the hover case, utilising flow visualisation techniques to obtain some empirical formulae for the position of both the tip vortex and the inboard sheet. Others, notably Cook (Ref [10]) and Caradonna and Tung (Refs [11 & 12]) have carried out extensive analysis on the structure and strength of tip vortices using curve fitting techniques, again for the hover case.

The forward ($90 < \psi < 270°$) and rear regions of the rotor are considered separately. This division is made because the velocity traces obtained in the forward zone

are, in general, reasonably straight forward to resolve into the various signatures. This contrasts with the rear region where the flow is considerably more complex and the determination of the various components which compound to form the velocity field is much more difficult.

6.1 The Forward Region of the Wake

Examination of the velocity data in this region reveals, in general, a well behaved repeatable flow, particularly in the tip region. The standard deviation of the samples at the same phase was typically < 5% indicating small rev. to rev. variations.

The dominant features in the flow are the blade bound vortices, with the trailing vortices becoming more pronounced as data from stations closer to the tip are inspected. For the case of $\mu = 0.1$ at $\Psi = 180°$ and at r/R = 0.8 (Fig [11]) with blade passes, the Y-component of flow reaches a minimum, the Z-component is changing between a maximum and a minimum and the X-component only shows minor changes. This phenomenon is consistent with the passage of a vortex lying approximately parallel to the blade, with the sense of the circulation in agreement with that required of the blade bound circulation. A simple lifting line model of the blade suggests that the variations of the Y-component about the blade passage should be symmetrical. This is not the case, a slight asymmetry being present which suggests that the effect of the chordwise distribution of the blade bound circulation is being detected.

The radial position of the tip vortex appears to lie between 0.95R and 1.0R. This is because these stations show the largest variation in the X-velocity component.

Similar trends are apparent for the rest of the data obtained in this forward region.

6.2 Tip Vortex Roll-Up

By examining the induced velocities measured at positions near the blade tip it is apparent that the roll-up is completed within ~5° behind the blade.

The velocity trace in the spanwise direction resulting from a semi-infinite trailing vortex originating from the blade tip would have the form ~(1-cos δ), where δ is the angle between a line joining the trailing edge of the blade to the probe and the vortex. However the data is plotted with respect to a timing pulse referenced to the blade 1/4 chord position which adds ~4° to δ.

The results obtained at 1.0R at all azimuth stations show a variation 5°-10° after the blade passage. The tip vortex is therefore not completely rolled-up as it leaves the trailing edge, but that the roll-up takes place rapidly and is complete within ≤ 5° of leaving the trailing edge. Corrections for the presence of tip vortices from previous blade passage and to convection in the free stream do not alter this conclusion.

Estimates of the strength of the tip vortex can be made from the velocity traces obtained from measuring stations in the tip region of the rotor assuming that the tip vortex is semi-inifinite.

Using this model together with assumptions that strength and radial position are constant in the vicinity of the probe permits the strength to be estimated to within 10% of the true value using the spanwise velocity data.

In a similar manner the effect on the chordwise flow during the blade passage is used to find the blade circulation. The assumption is made that the circulation of the blade is constant in the spanwise direction, but this leads to some error as the blades were not

ideally twisted. The error of such an assumption has been assessed for the particular configuration tested and results in an error of less than 3% in the tip region.

To obtain an estimate of the blade circulation the magnitude of the velocity it induces must be made. This is found by assuming that when the blades are far away from the probe position ($\pm 45°$) the contribution of the bound circulation to $V_{chordwise}$ is negligible and when the blade is directly overhead of the probe its contribution is a maximum.

These calculations are made for each radial probe position and give an estimate of the maximum circulation Fig [12]. Fig. [13] shows the value of the tip vortex strength obtained by the method described in the previous section, represented as a percentage of the maximum blade circulation at the appropriate azimuth.

This simple analysis was extended by a least squares curve fitting programme using the following parameters: local blade circulation, tip vortex strength, radial position of the tip vortex and a velocity vector representing all effects contributing to the flow not explicity included in the above list.

A schematic of the simple mathematical model of the blade is shown in Fig [14]. Blade flapping was considered important and was input from the data obtained from the blade strain gauges mentioned in section 2.4.

The analysis was a least squares fit in seven variables which used data from the reference position and from 10 surrounding positions (i.e. within a sector of $\psi \pm 15°$ about the reference position).

Only the values obtained for the total blade circulation proved to be useful since it was found that, although the two vortex model gave a better fit to the data, the distribution of the vorticity between the two yielded no useful information. This was somewhat disappointing since it had been hoped initially that this would provide an estimate, albeit crude, of the pitching moment.

Figs [15 and 16] show typical results. A typical comparison of the velocities calculated from the fitted parameters with the experimental data is shown in Fig [17].

The results obtained for the blade and tip vortex circulation confirmed the values obtained by the previous method, except at $\Psi = 150°$. They also give consistent values for the radial position of the rolled up tip vortex Fig. [17] which lies between 0.97-1.0R. The one value which does not fall in this region was obtained at $\Psi = 150°$, 0.95R, and gave a position of ~0.93R. All the evidence from other analyses coupled with the marked increase in higher order bending measured at outboard positions at $\psi = 150°$ suggests that the blade Ψ is passing close to the tip vortex from the preceding blade. Outboard of this there will be an upwash which will have the effect of increasing the local angle of attack and, hence, circulation. Since this applies a "peaky" load distribution the outboard bending moments will show an increase.The effect of this other vortex on the curve fitting programme at a measuring station which is heavily influenced by the preceding and current tip vortices will lead to the situation where the radial position is inaccurately estimated since the program only takes account of one vortex. This is also likely to account for the discrepancy observed in the estimated strength of the tip vortex at this position.

Bearing this in mind it is possible to draw the following conclusions from the results obtained;

A. The strength of the tip vortex lies in the range 0.9-1.1 x maximum blade circulation,

B. The radial position of the tip vortex after roll-up is in the region 0.97-1.0R.

Conclusion A above supports the findings of Cardonna and Tung (Ref [12]) since, bearing in mind the simplifying assumption made, the range obtained is conducive to the conclusion that the strength of the tip vortex is equal to the maximum blade circulation.

Conclusion B is in general agreement with the results of the determination of the wake structure obtained by Landgrebe (Ref [8]).

It is worth noting is that the difference between one blade and the other three can be clearly seen in the results.

6.3 The Rear Region of the Wake

The wake in the rear region of the rotor, is more complicated than in the forward region. Two phenomena are detected which make the simple analysis method developed for the forward region inapplicable. These are the blade thickness and the turbulent wake of the blade.

Aft of the rotor the simplicity of the wake structure is largely restored. The dominant feature here is the large induced velocities caused by the blade tip vortices as they are convected downstream, close to the position of the hot-wire probe position.

The boundary between the two different regions lies in approximately the place where the mean value of the flow Z-component changes from an upwash to a downwash. Thus, measurement stations in the rear are measuring the flow after it has passed through the rotor, hence, leading to the more turbulent nature of the flow which is in general observed.

Figure [18] shows a representative result obtained at $\Psi = 0°$, $\mu = 0.1$, r/R, 0.95. By analogy with the forward region at inboard positions a minimum in the chordwise component was expected at the blade passage, with the vertical component changing from a maximum to a minimum due to the blade bound vortex. At outboard stations the effect of the tip vortex becomes more pronounced with a consequent increase in the spanwise component of flow after the blade passage. This is broadly what is observed, with two significant additions, the peaks labelled A and B on Figure [18]. Peaks A is a pronounced dip in the chordwise velocity component, indicating an increase in the velocity in the direction of the blade motion, and at the same time a considerably smaller increment observed in the vertical component, with virtually no change occuring in the spanwise component. Similar peaks show up on the majority of results obtained in the rear region. One of the important attributes of these is that the time at which they occur, relative to the blade passage, varies considerably between different measuring stations. This is discussed further in Section 6.5.

Peaks B on Figure [18] are phase locked to the blade, occuring almost immediately after the blade passage. The changes in chordwise and vertical flow components are in the sense opposite to that which would be expected from the blade vorticity. The effect was traced to the blade thickness by calculating the change in probe velocity due to an appropriate potential flow model of the blade. General agreement was obtained.

In the tip region the chordwise component of the flow behaves in much the same way as was previously observed, reinforcing the conclusion that the roll-up of the trailing vorticity is rapidly completed.

The cause of the peaks A Figure [18] was more difficult to track down, since the phase varied markedly between measuring stations.

To obtain more information about the phenomenon, the size of the peaks above the local background level was measured at all positions at which they were apparent.

The magnitude and direction of the maximum velocity increment found in each of the peaks was then plotted (for the X-Y) plane, in Figure [19]. While the phase of the signal varied markedly between measuring stations the direction of the increments was consistent, being almost parallel to that of the blade motion as it passed overhead of the probe.

The standard deviation of the velocities at $\mu = 0.1$, $\Psi = 0°$ e.g. Fig. [20] shows a marked increase at the velocity peaks. A hypothesis that the turbulent wake of the blade was being detected was formed. To test this it was assumed that the cause of the velocity peaks was convected downstream with the appropriate mean velocity measured at the appropriate measuring station. The position and time at which this would have occured at the rotor plane was then calculated by using the mean value of the Z-component and the separation of the probe from the rotor plane to calculate the time (t_o) taken for the phenomenon to traverse this distance. The X and Y coordinate of the intersection with the rotor plane were then calculated using t_o and the appropriate mean velocity values. The blade position at time t_o was also obtained. A good agreement between the blade position and the extrapolated position of origin of the disturbance was found Fig. [21] which supported the hypothesis.

The reason why the velocity increment due to the turbulent wake appears as an enhancement in velocity, instead of the deficiency that would normally be expected, is due to the reference frame in which the measurements are made. In conventional wind tunnel measurements the aerofoil and probe are at rest w.r.t. each other thus, outside of the wake (far downstream) the probe would detect the free stream velocity but inside the wake there would be a reduction in the velocity. In the present case the situation is different. If we consider a reference frame fixed to the blade, then (neglecting the velocity component due to the forward motion of the helicopter) the velocity of the airflow outside the wake w.r.t. the blade is -V and inside the wake will be -(V-dv). However, since the probe itself is also moving with velocity -V w.r.t. the blade it follows that outside the wake the probe will sense zero velocity. Inside the wake the velocity sensed will then be -(V-dv) - (-V) i.e. dv, a positive increment.

6.4 Determination of Blade Profile Drag

An attempt to estimate the blade profile drag was made. It ws assumed that (1) the static pressure across the wake was constant, and (2) the freesteam velocity U_∞ is the linear velocity of the blade at the appropriate radial station plus the chordwise component of rotor forward speed at the corresponding azimuth

The estimates of the local blade profile drag are shown in Table [5];

NOTE: In the above table the columns labelled probe refer to the probe position where the data was collected. Those labelled blade refer to the calculated position of the blade when the wake measured was shed.

It is clear that these values are in the range that would be expected for a NACA 0015 aerofoil operating at moderate angles of attack. This further supports the hypothesis made.

The effect of the velocity peaks due to the profile drag of the main rotor blades on the tail rotor is a question which must be posed.

The above measurements of the blade wake also support the theoretical work of Fogarty and McCroskey et al which indicates that the spanwise flow in the blade boundary layer should be small, particularly for turbulent boundary layers. This is clearly indicated in the data obtained, where the flow in the turbulent blade wake has no significant component in the spanwise direction.

TABLE 5: Values of Profile Drag

PROBE AZIMUTH	PROBE r/R	BLADE AZIMUTH	BLADE r/R	Cd
0	0.80	358	0.68	0.0145
	0.90	359	0.78	0.0138
	0.95	359	0.84	0.0142
	1.0	360	0.89	0.0158
15	0.95	17	0.84	0.0152
	1.0	16	0.89	0.0167
30	0.9	34	0.80	0.0144
	0.95	34	0.86	0.0158
	1.0	34	0.91	0.0157
60	0.6	73	0.53	0.0124
	0.8	67	0.75	0.0166
	0.9	65	0.85	0.0130
300	0.8	289	0.73	0.0107
	0.9	293	0.82	0.0095
	0.95	296	0.87	0.0136
330	0.8	318	0.59	0.0030
	0.9	322	0.75	0.0060
	0.95	324	0.81	0.0133
	1.0	325	0.88	0.0153
345	0.95	341	0.82	0.0098
	1.0	342	0.87	0.0129

6.5 The Wake Aft of Rotor Disc

The wake aft of the rotor disc, particularly between Ψ = 330° and Ψ = 30° shows considerable evidence of strong vortex activity. This effect is most pronounced w.r.t. the spanwise and vertical components, the variations in the chordwise component being much smaller. The implication of this, taking into account the shape of the velocity trace, is that it is caused by the close passage of strong, concentrated vortices approximately parallel to the chordwise axis.

These are the rolled-up tip vortices. The maximum measured velocty occurs at μ = 0.1, ψ = 15° and r/R = 1.1, Fig. [22] with the magnitude diminishing at positions further outboard. The time relative to the blade passage at which the velocity peaks occur become successively greater, the phase change being about 20° for a change in r/R of 0.05. At 2500

r.p.m. 20° corresponds to a time of about 1.35×10^{-3} seconds which implies an X-component of flow of about 25m/s, which is in reasonable agreement with the mean X-component measured at this position.

According to Andrew (Ref [13]) the core size of trailing vortices has been variously reported as lying anywhere in the range r/c = 0.016-0.079. The H.S.R. rig, has a chord of 6cm this leads to a calculated core size of 9.6×10^{-4} - 4.7×10^{-3}m. The active portions of all 3 wires of the probe are mounted in a sphere 3×10^{-3}m in diameter. It is, therefore, obvious that such a probe cannot give detailed information about the structure of the vortex core. Due to the finite size of the probe, when a vortex approaches closely, the large velocity gradients could mean that the wires are not all measuring the same effective flow field. This would lead to inaccuracies in the determination of both magnitude and direction of the flow.

Examining traces for individual rotor revolutions indicates that the maximum tangential velocity (Vs/Vt) is about 0.15. This figure is low in comparison to that reported elsewhere. However, in view of the above instrumentation limitations this should be regarded as being a lower bound. An upper bound on the core size of the vortex can also be obtained by measuring the time taken for the induced velocity to change from a maximum to a minimum. Typically, this time is between 4×10^{-4} - 8×10^{-4} seconds. This leads to a core diameter of about 5×10^{-3} - 1.2×10^{-2}m or r/c = 0.083-0.2. These figures being somewhat on the high side to those reported elsewhere.

During a vortex strike on the probe there is a marked trough in the chordwise component. This suggests that there is an axial flow in the vortex core, moving towards the blade. This agrees with a result previously reported by Widnall and Bliss (Ref [14]) in connection with results obtained during full scale flight tests on fixed wing aircraft.

This being the case the accuracy of vortex core measurements obtained by use of single hot-wires, such as those of Carradonna and Tung et al (Refs [11 and 12]) could be questioned. They have attempted to minimise the error due to the axial flow by mounting the wire parallel to the core (in itself raising the question of how the orientation of the core in relation to the probe is known). However the cooling velocity sensed by the wire will not be solely due to the induced tangential velocity of the core plus the convection velocity.

7.0 CONCLUSIONS

The research program described in this report has shown that it is possible to obtain good time varying data for the velocity field in the vicinity of a lifting rotor using triaxial hot-wire probes. Using the measuring technique developed an extensive map of the flow in one plane beneath the rotor has been obtained and this has provided a much needed increase in the available data on rotor wakes. This is an area, as the literature reveals, where previously only limited information was available.

Analysis of the data obtained has provided considerable information about the behaviour of the rotor wake and the full conclusions drawn are outlined in detail in the next section.

The conclusions reached are;

A. A velocity measuring technique, using tri-axial hot-wire probes, has been developed which is accurate to within ± 2% in magnitude and ± 2° in yaw and pitch.

B. The value of K generally used in the Glauert induced velocity formula is too low by about 50%.

C. At all positions in the wake where the flow was sufficiently steady to obtain acceptable data the frequency spectrum of the velocity data is composed of frequencies which are multiples of the rotor frequency.

D. Analysis of the velocity data can be used to track down small differences in the characteristics of blades.

E. The roll-up of the tip vortex takes place rapidly and is substantially complete within 5° azimuth after the blade passage.

F. The radial position of the tip vortex after roll-up is in the range 0.97-1.0R.

G. The strength of the tip vortex is approximately equal to the maximum bound circulation.

H. There are significant differences at certain positions in the wake in both the time varying and time average data obtained at the same advance ratio, but different tip speed. This is most marked in data from the 4th quadrant. If these areas are important in model scale experiments run at reduced r.p.m. then scaling to full scale tip speed could be misleading.

I. The existance of sharp edged "gusts" due to the turbulent blade wake has been shown and these may have significant effects on tail rotor noise and vibratory load during certain flight conditions.

J. Reasonable estimates of the blade profile drag can be made from those velocity measurements which show clear evidence of the turbulent blade wake.

K. There is no significant spanwise velocity component in the turbulent blade wake.

L. An upper limit for the radius of the vortex core of r/c = 0.2 has been obtained.

M. The existance of axial flow in the tip vortex core toward the blade has been shown.

8.0 REFERENCES

1. F.E. Jorgensen: "Directional Sensitivity of Wire and Fibre-Film Probes". DISA Information, No. 11 May 1971.

2. G.D. Huffman: "Calibration of Triaxial Hot Wire Probes Using a Numerical Search Algorithm". J Physics E Sci Instrum, Vol. 13; 1980.

3. H.R.Velkoff, R. Nararro and H.Terkel: "Measurement of the Instantaneous Velocities in a Helicopter Rotor Wake in Forward". Ninth European Rotorcraft and Powered Lift Aircraft Forum , Paper No. 1; 1983.

4. H.H. Heyson and S. Katzoff: "Induced Velocities Near a Lifting Rotor with Non-Uniform Disk Loading". NACA Report 1319; 1956.

5. J.H. Spreito and A.H. Sachs: "The Rolling Up of the Trailing Vortex Sheet and its Effects on the Downwash Behind Wings". Jou Aero Sci, Vol 18, No. 1 Jan 1951.

6. H. Glauert: "A General Theory of the Autogyro". ARC R & M , No. 1111; 1926.

7. R.P. Coleman, A.M. Feingold and C.W. Stempi: "Evaluation of the Induced Velocity Field of an Idealized Helicopter Rotor". NACA WR L-126, 1945 (Formerly NACA ARR L5E10).

8. A.J Landgrebe: "The Wake Geometry of a Hovering Helicopter and Its Influence on Rotor Performance". Journal of the American Helicopter Society, Vol. 17, No. 4; 1972.

9. A.J. Ruddell: "Advancing Blade Concept (ABC tm) Development". 32nd Annual National Forum of the American Helicopter Society; 1976.

10. C.V. Cook: "The Structure of the Rotor Blade Tip Vortex". Westland Helicopters, Research Paper, No. 430; 1972.

11. C. Tung, S L. Pucci, F.X. Caradonna and H.A. Morse: "The Structure of Trailing Vortices Generated by Model Rotor Blades". Seventh European Rotorcraft and Powered Lift Aircraft Forum, Paper No. 4; 1981.

12. F.X. Caradonna and C. Tung: "Experimental and Analytical Studies of a Model Helicopter Rotor in Hover". Vertica, Vol. 5 1981.

13. M.J. Andrew "Co-Axial Rotor Aerodynamics in Hover". Vertica, Vol. 5; 1981.

14. S.E. Widnall and D.B. Bliss: "Slender-Body Analysis of the Motion and Stability of a Vortex Filament Containing Axial Flow". J Fluid Mech, Vol. 50; 1971.

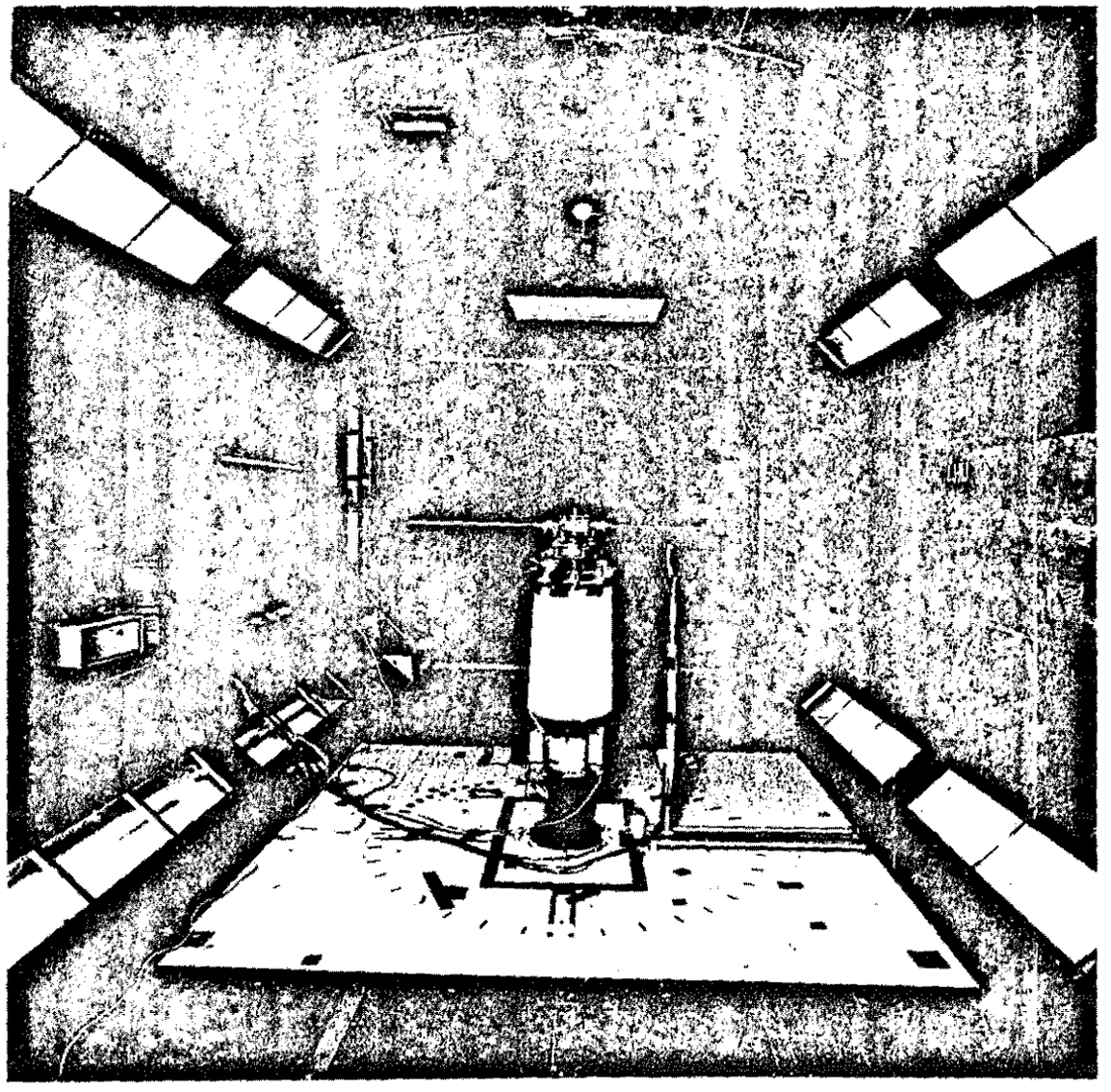

Figure 1 Photograph of rotor installed in 11 x 8ft wind tunnel

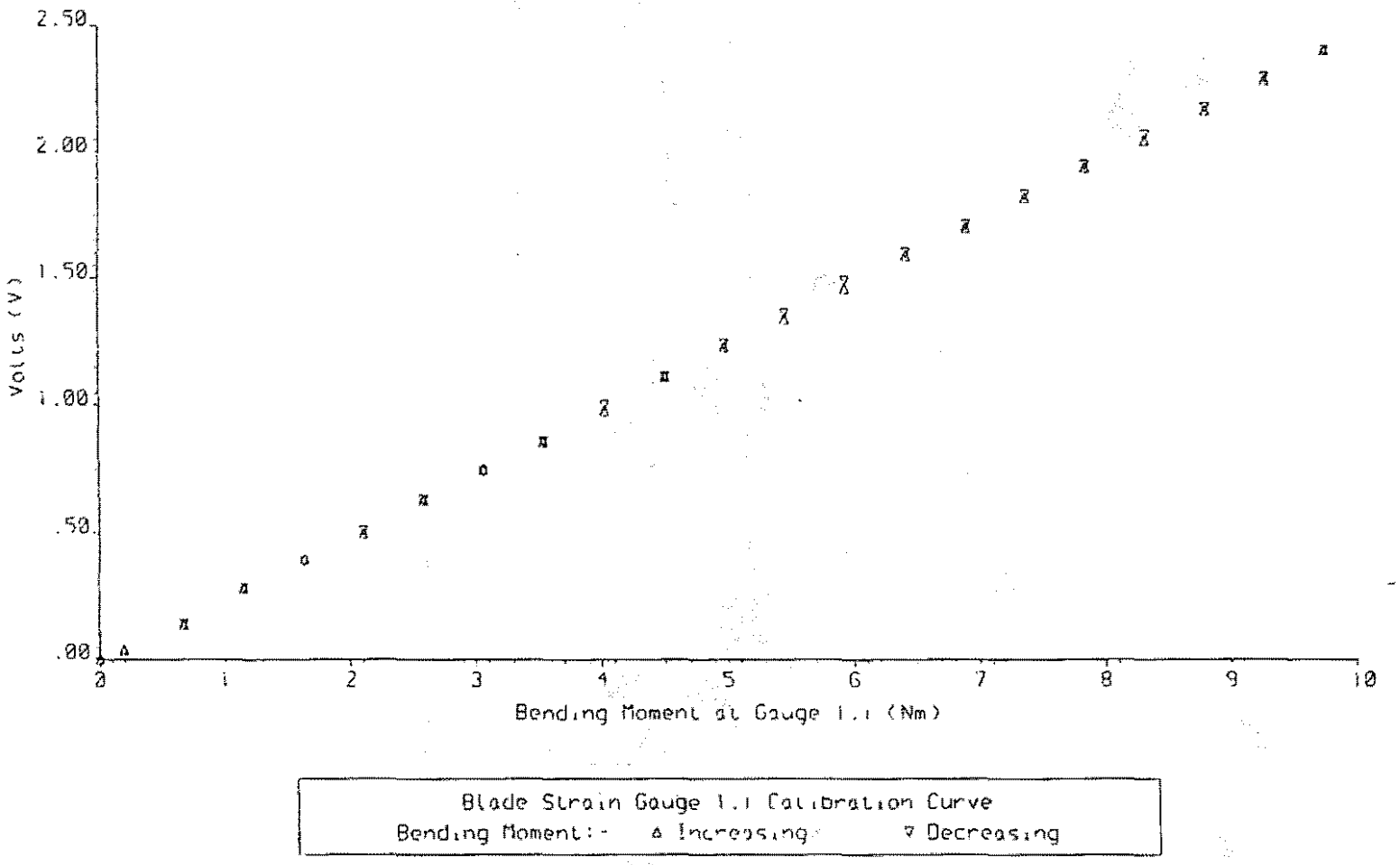

Figure 2
Typical Calibration Curve for Blade Strain Gauges.

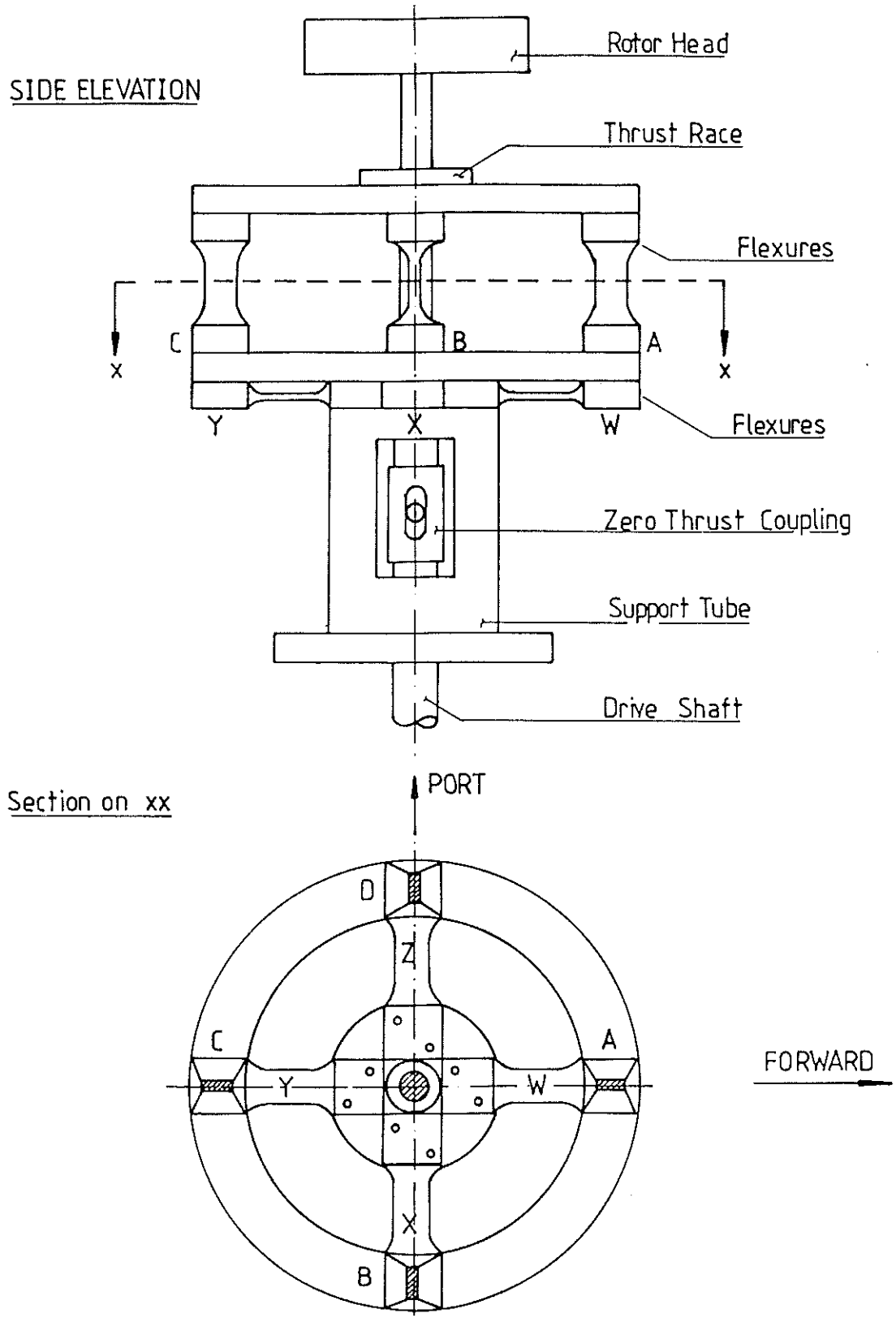

Figure 3
Schematic of Balance Arrangement (From Ref [35]).

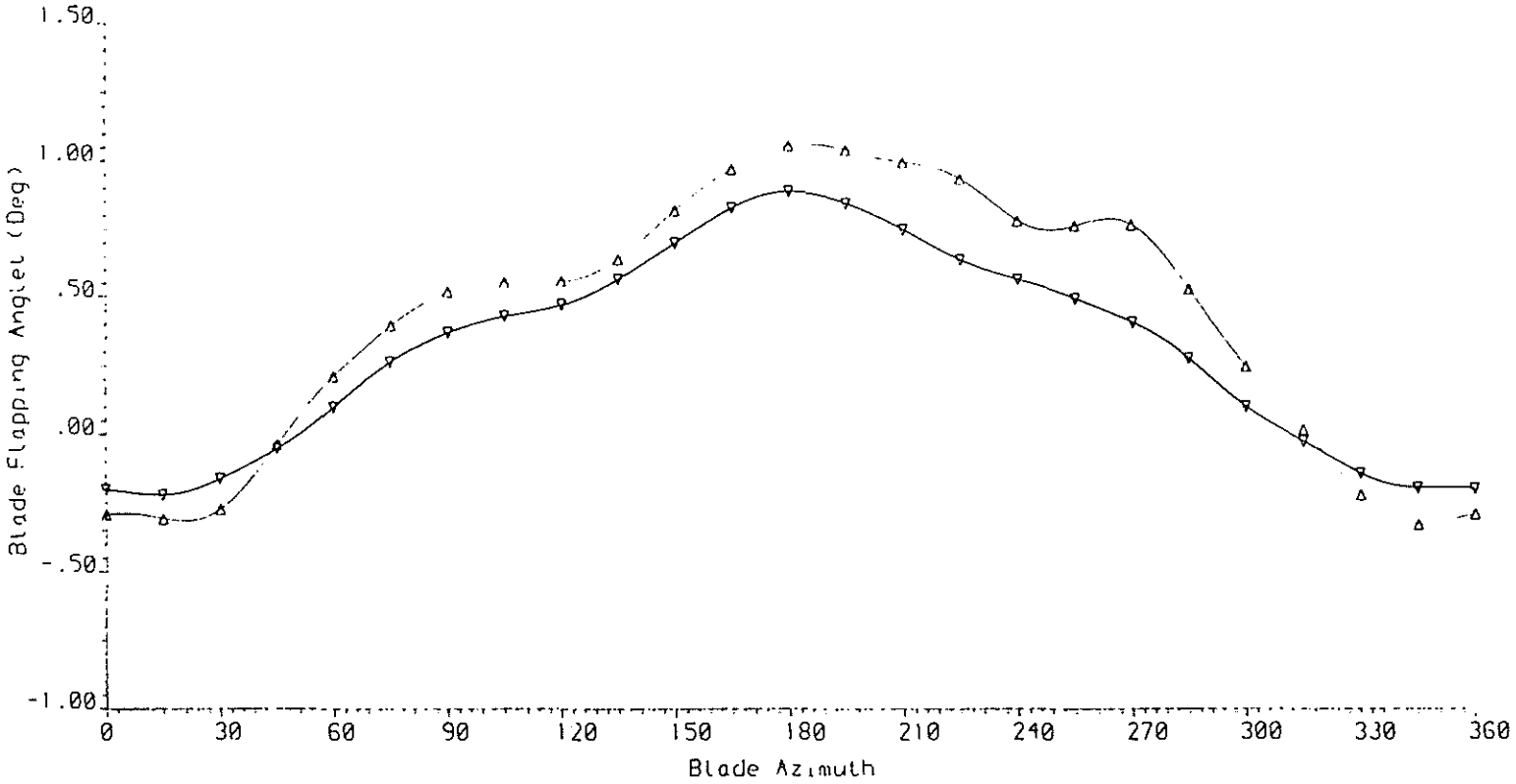

Adv Ratio= 0.100 Rotor RPM= 2500.0	Flapping angle obtained from 3 modes Symbol △ plotted every 15 degrees
Adv Ratio= 0.100 Rotor RPM= 2500.0	Flapping angle obtained from 1 modes Symbol ▽ plotted every 15 degrees

Figure 4

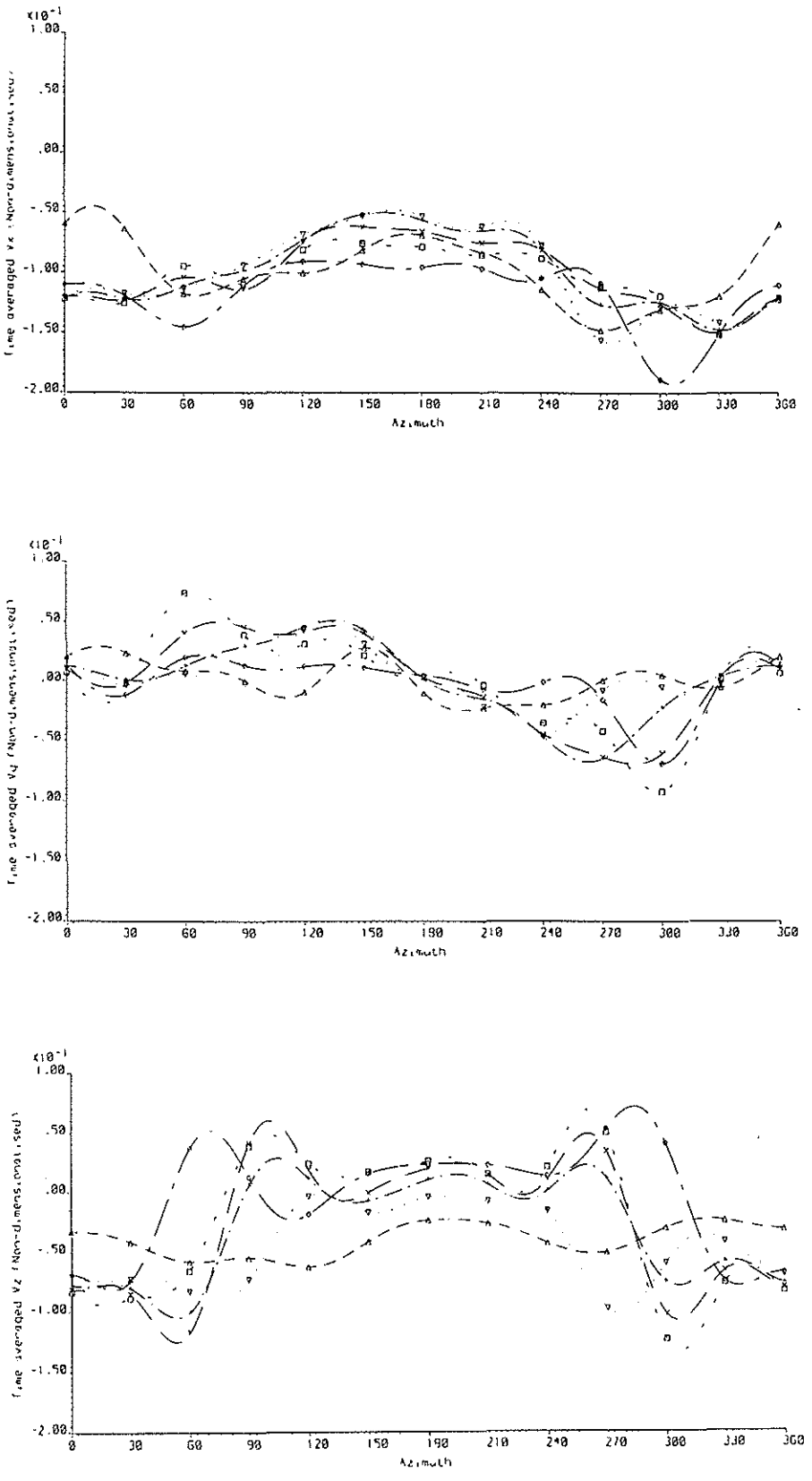
x10⁻¹
1.00
.50
.00
-.50
-1.00
-1.50
-2.00
0
30
60
90
120
150
180
210
240
270
300
330
360
Azimuth
Plot of non-dimensionalised time averaged values of Vz
Advance ratio=0.100
R.p.m.=2500
Data From 0.6R
Data From 0.9R
Data From 1.0R
Data From 0.95R
Data From 1.1R

Figure 5

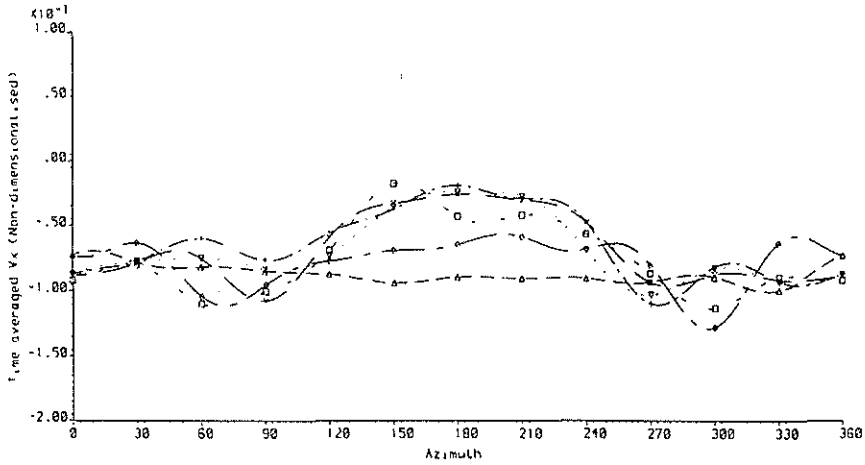

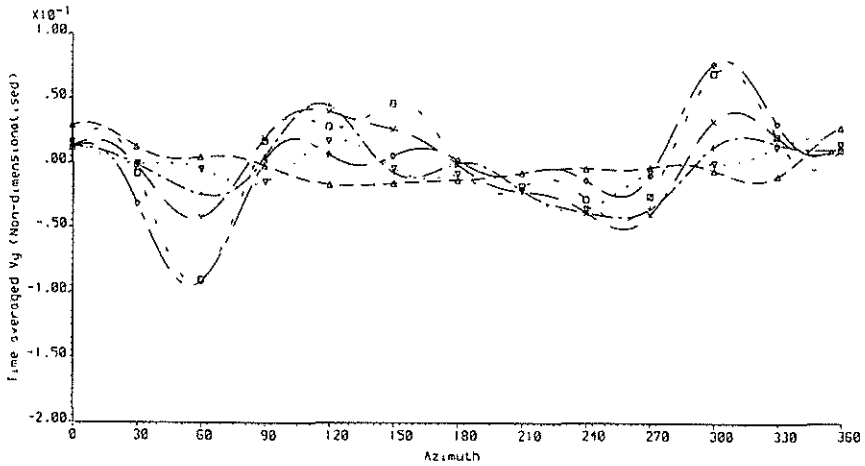

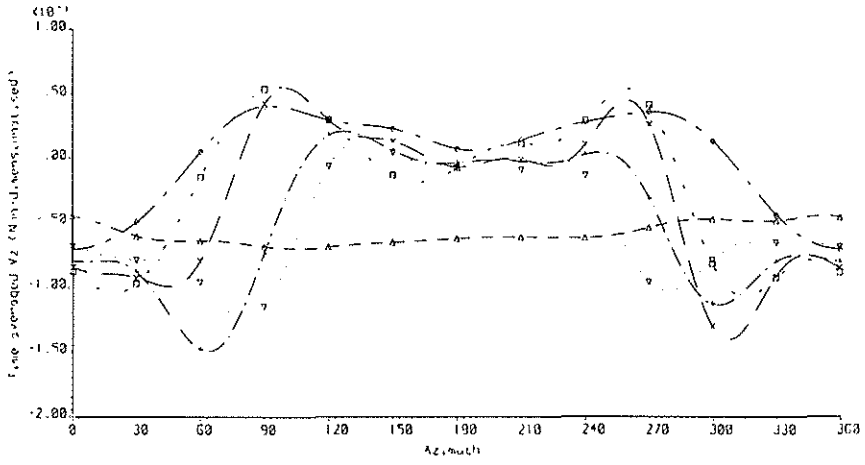

Plot of non-dimensionalised time averaged values of Vz
Advance ratio=0.067 R.p.m.=1250
Data from 0.5R
Data from 0.9R
Data from 1.0R
Data from 0.9R
Data from 0.95R
Data from 1.1R

Figure 6

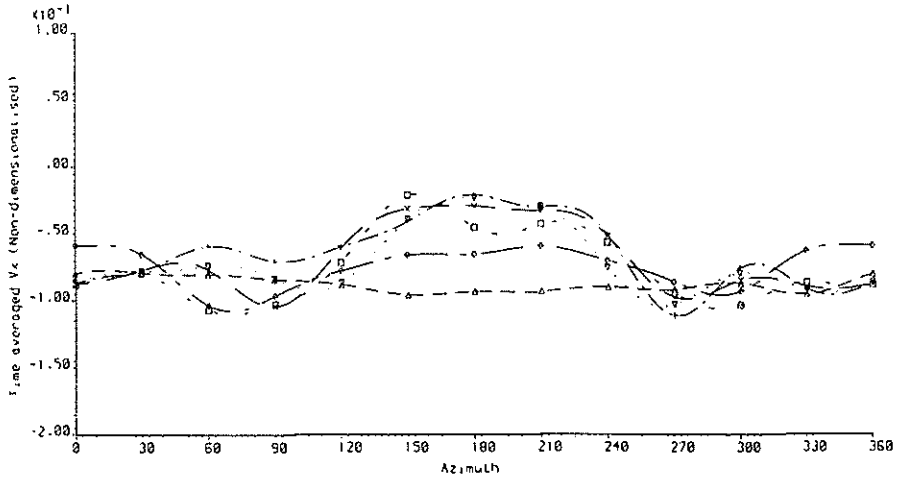
x10⁻¹
1.00
.50
.00
-.50
-1.00
-1.50
-2.00
Time averaged Vx (Non-dimensionalised)
0
30
60
90
120
150
180
210
240
270
300
330
360
Azimuth

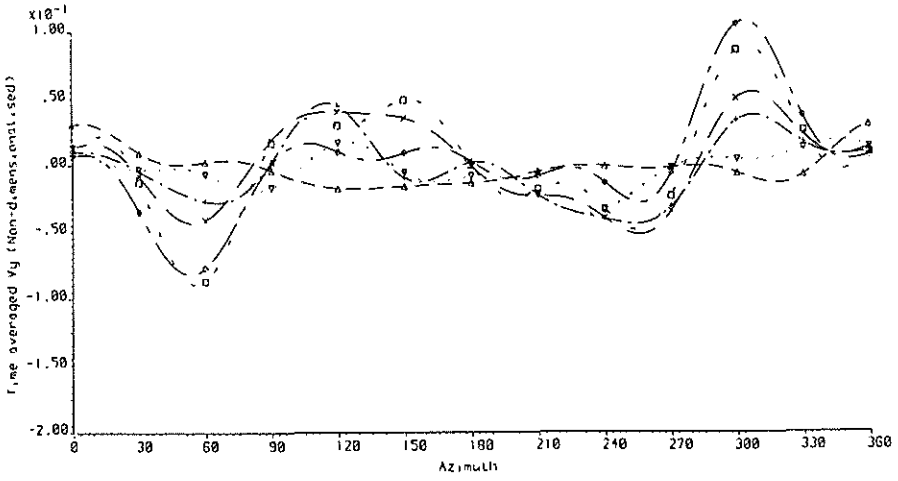
x10⁻¹
1.00
.50
.00
-.50
-1.00
-1.50
-2.00
Time averaged Vy (Non-dimensionalised)
0
30
60
90
120
150
180
210
240
270
300
330
360
Azimuth

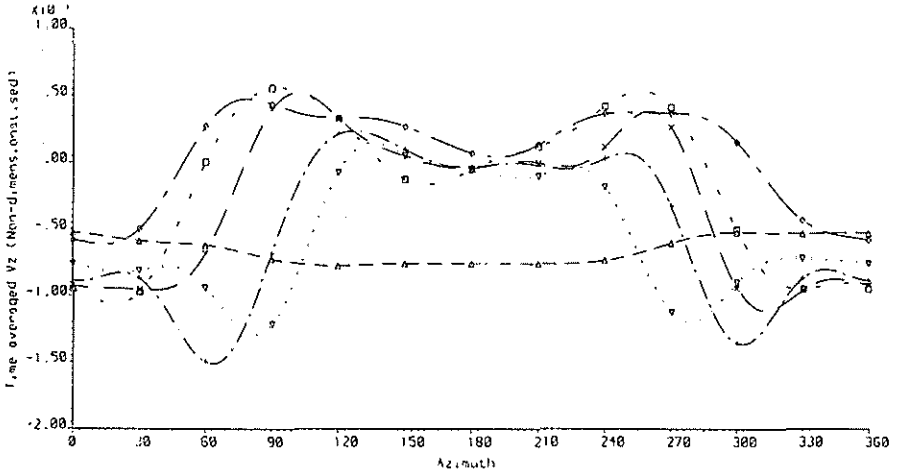
x10⁻¹
1.00
.50
.00
-.50
-1.00
-1.50
-2.00
Time averaged Vz (Non-dimensionalised)
0
30
60
90
120
150
180
210
240
270
300
330
360
Azimuth

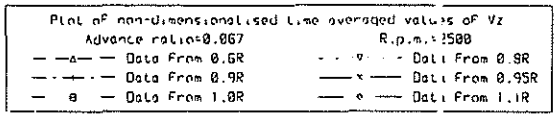
Plot of non-dimensionalised time averaged values of Vz
Advance ratio=0.067
R.p.m.=2500
Data From 0.6R
Data From 0.8R
Data From 1.0R
Data From 0.9R
Data From 0.95R
Data From 1.1R

Figure 7

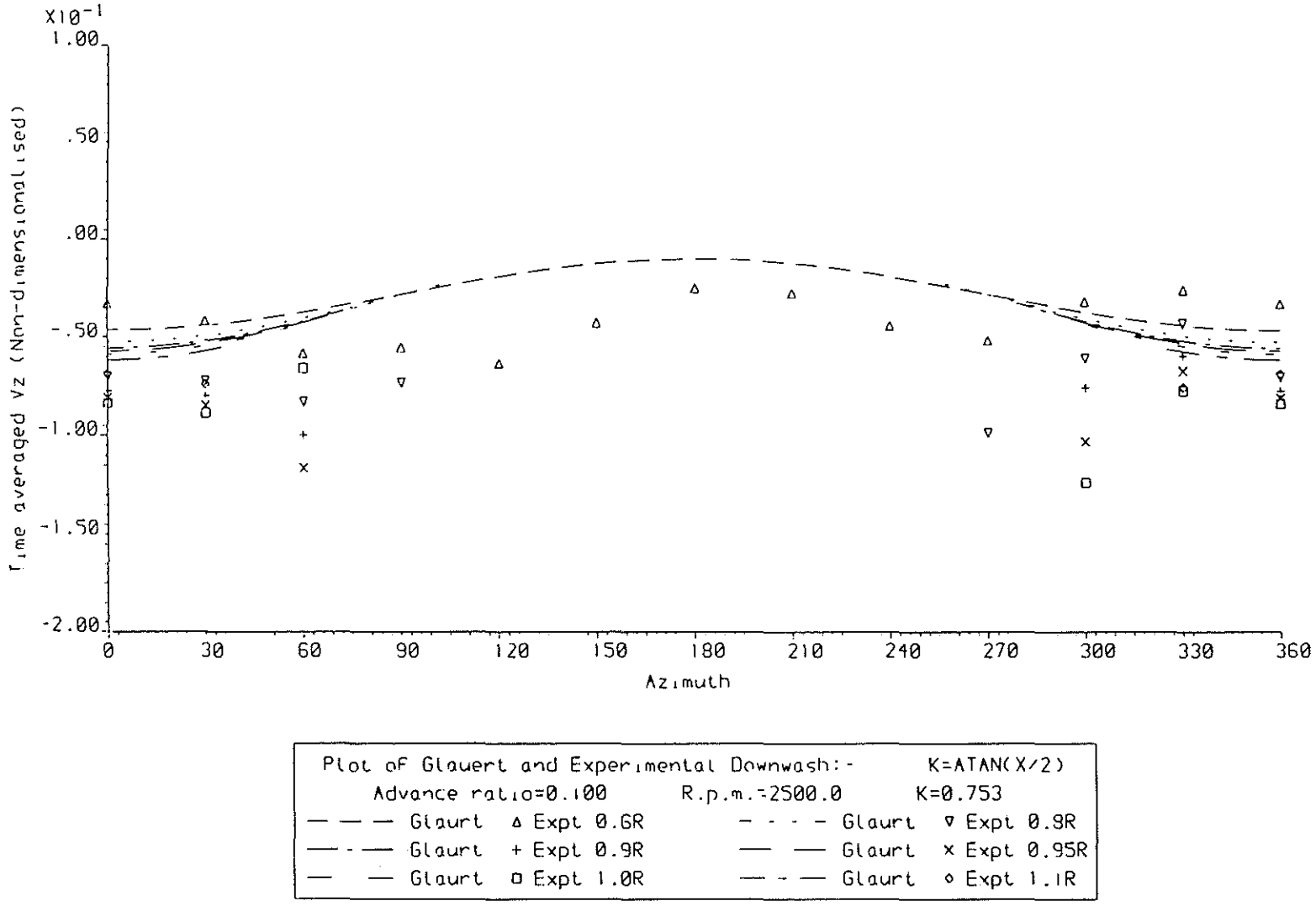
X10⁻¹
1.00
.50
.00
-.50
-1.00
-1.50
-2.00
Time averaged Vz (Non-dimensionalised)
0
30
60
90
120
150
180
210
240
270
300
330
360
Azimuth
Plot of Glauert and Experimental Downwash:-
K=ATAN(X/2)
Advance ratio=0.100
R.p.m.=2500.0
K=0.753
Glauert
Expt 0.6R
Glauert
Expt 0.8R
Glauert
Expt 0.9R
Glauert
Expt 0.95R
Glauert
Expt 1.0R
Glauert
Expt 1.1R

Figure 8

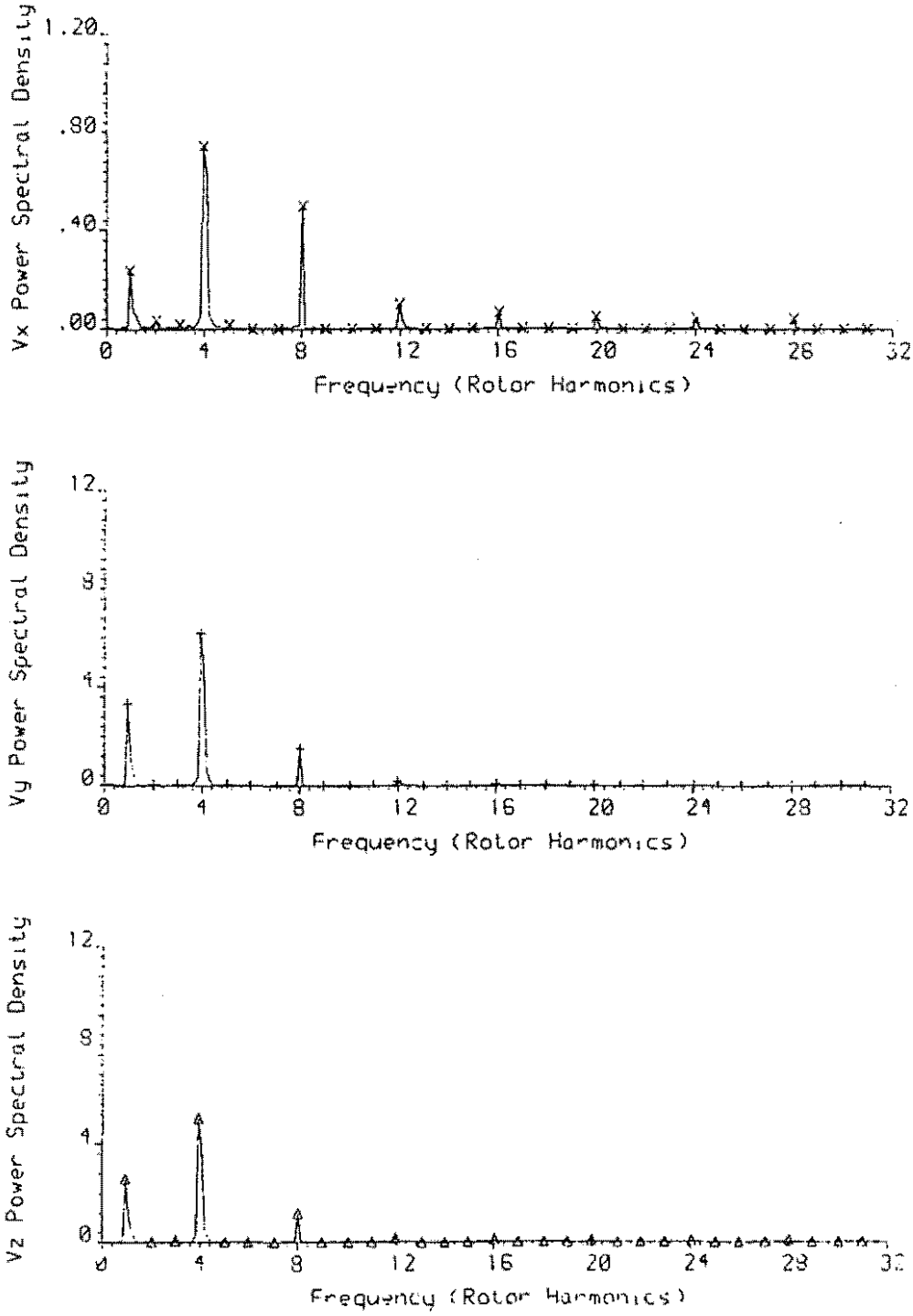
Vx Power Spectral Density
1.20
.80
.40
.00
0
4
8
12
16
20
24
28
32
Frequency (Rotor Harmonics)
Vy Power Spectral Density
12
8
4
0
0
4
8
12
16
20
24
28
32
Frequency (Rotor Harmonics)
Vz Power Spectral Density
12
8
4
0
0
4
8
12
16
20
24
28
32
Frequency (Rotor Harmonics)
Probe Azm= 270.0
Rotor RPM= 2450.2
× X-compt
Probe z/R=-0.075
Adv Ratio= 0.106
+ Y-compt
Probe r/R= 1.000
△ Z-compt
Symbols plotted at harmonics of rotor frequency

Figure 9

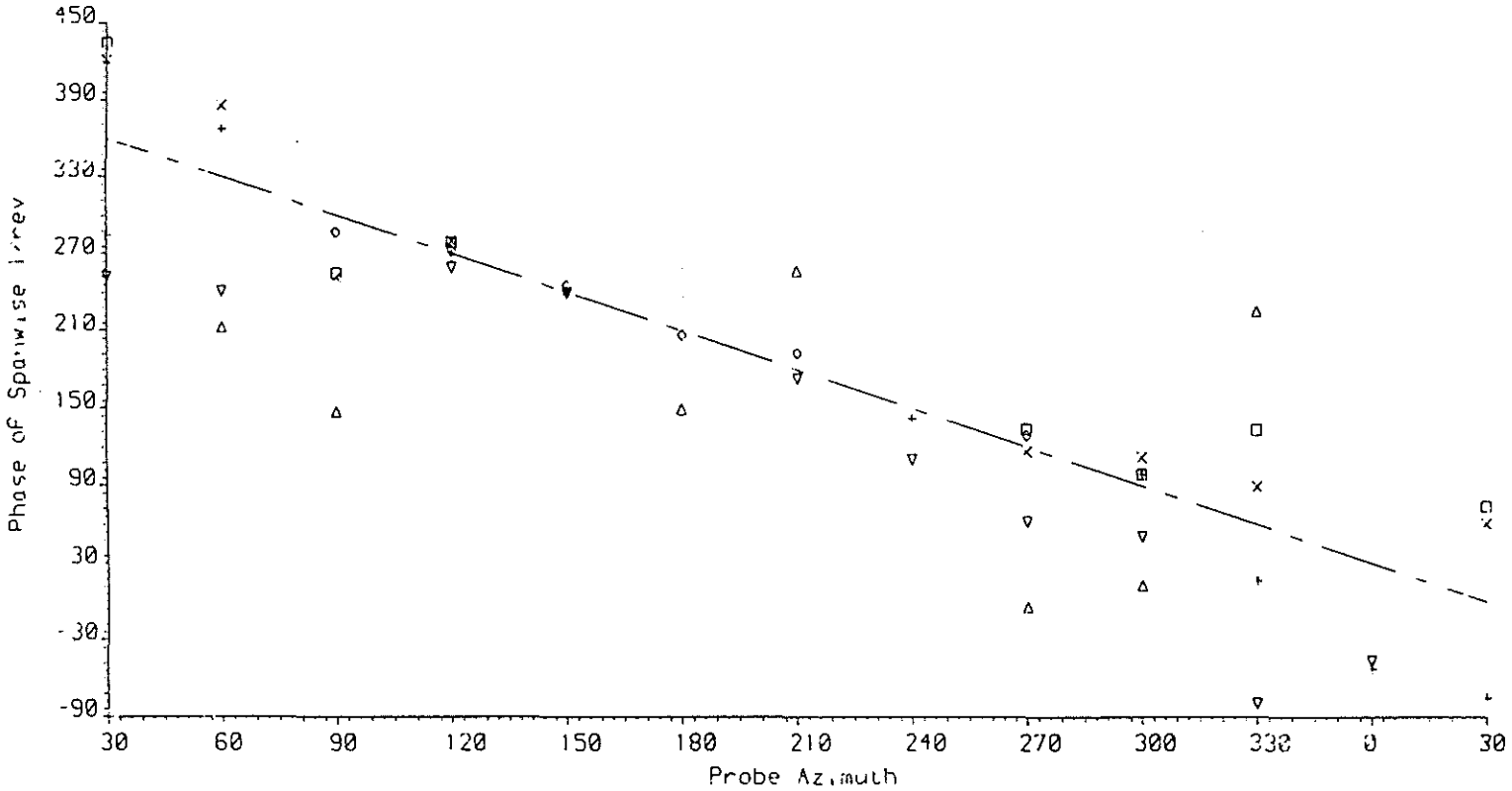

Plot of phase of Spanwise 1/rev against probe azimuth	
Advance ratio=0.100	R.p.m.=2500
△ Data from 0.6R	▽ Data from 0.8R
+ Data from 0.9R	× Data from 0.95R
□ Data from 1.0R	◇ Data from 1.1R

Figure 10

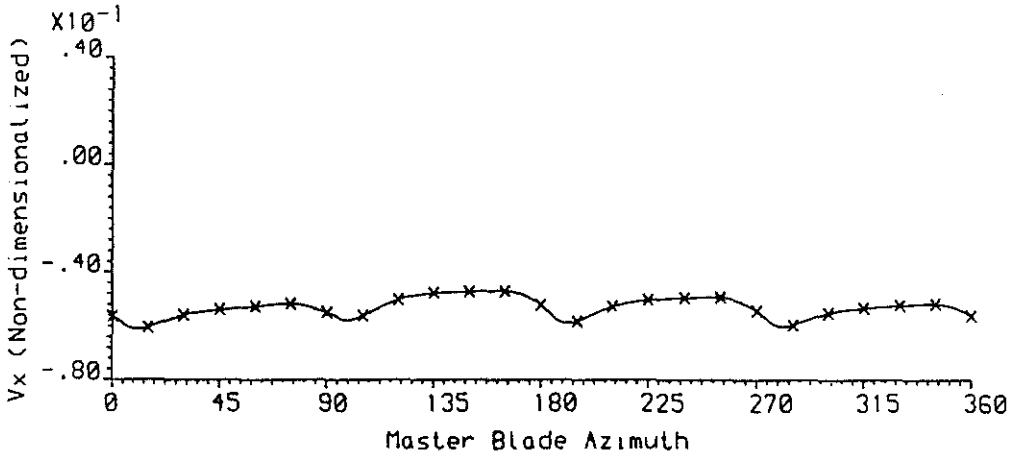

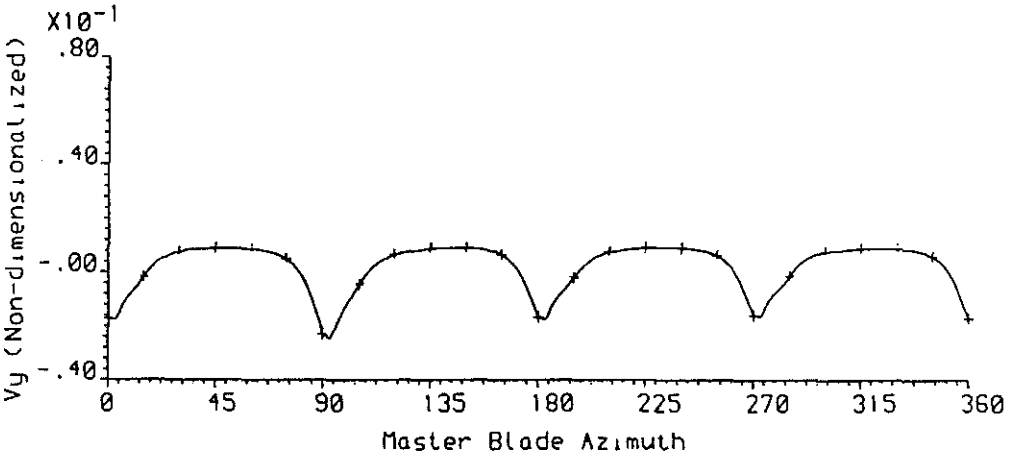

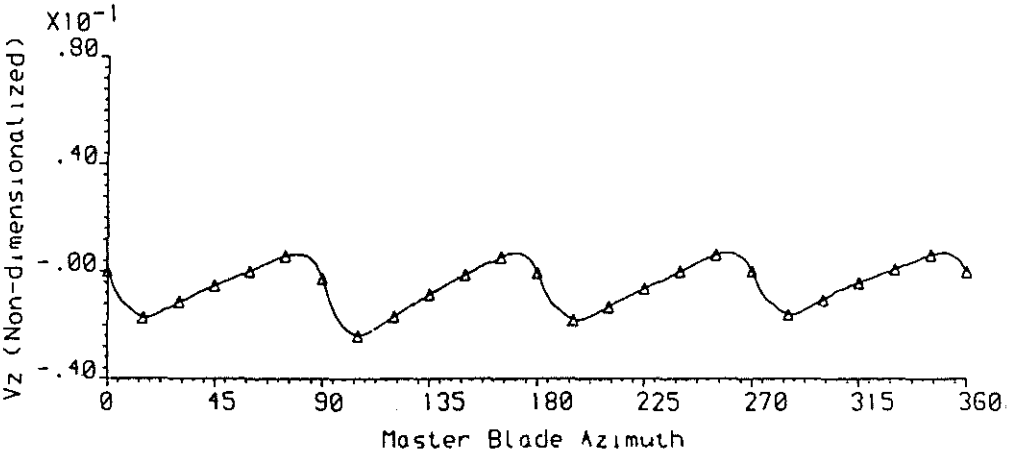

Probe Azm= 180.0	Rotor RPM= 2500.7	× X-compl
Probe z/R=-0.075	Adv Ratio= 0.107	+ Y-compl
Probe r/R= 0.800	Revs Avgd= 32	△ Z-compl
Symbols plotted at 15 degree intervals		

Figure 11

Figure 12

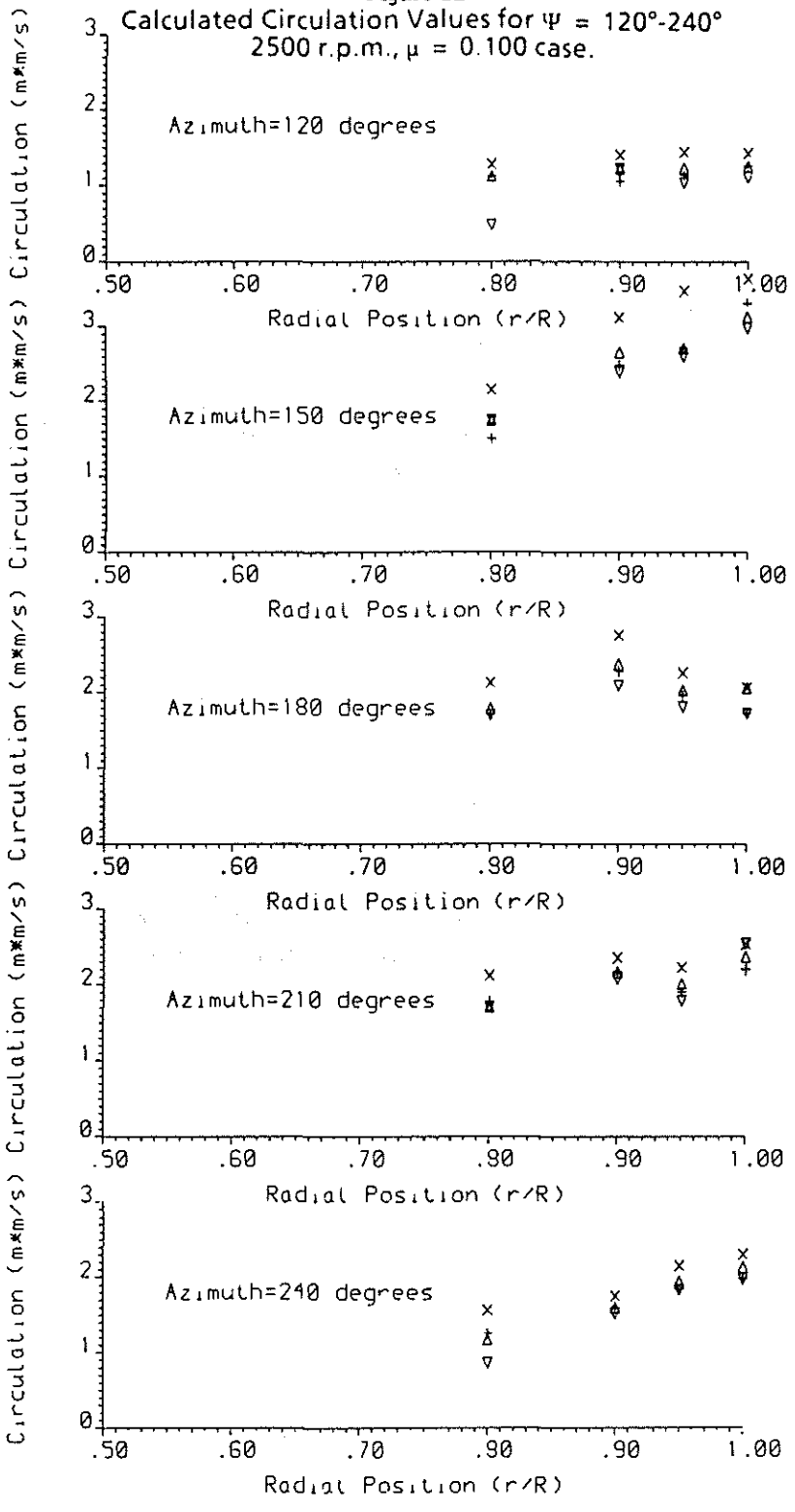
Calculated Circulation Values for Ψ = 120°-240°
2500 r.p.m., μ = 0.100 case.
Azimuth=120 degrees
Azimuth=150 degrees
Azimuth=180 degrees
Azimuth=210 degrees
Azimuth=240 degrees
Radial Position (r/R)
Circulation (m*m/s)
.50
.60
.70
.80
.90
1.00
0
1
2
3
Plot of circulation against radius
Blade 1
Blade 2
Blade 3
Blade 4

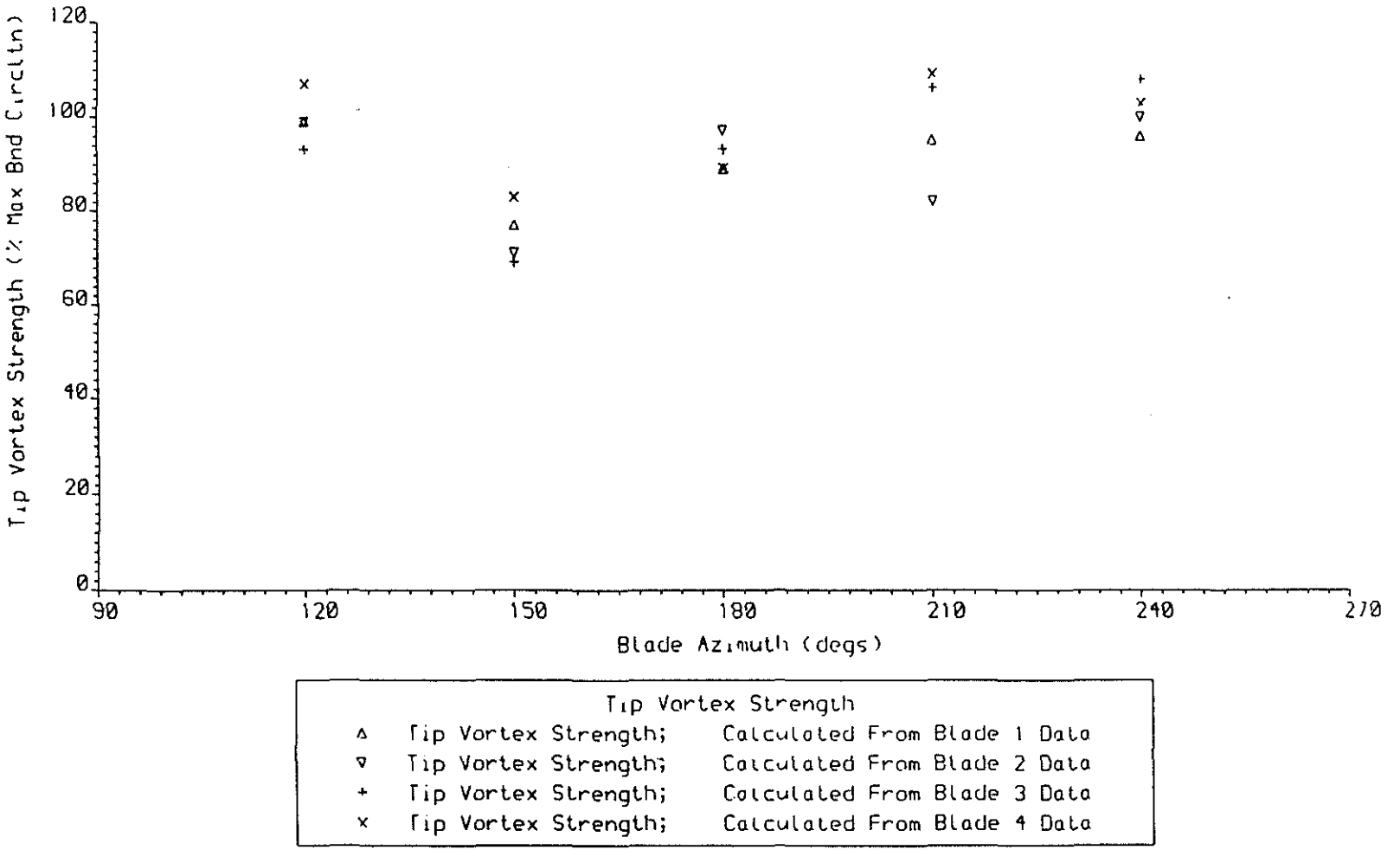

Figure 13
Calculated Tip Vortex Strength for Ψ = 120°-240°
2500 r.p.m., μ = 0.100 case.

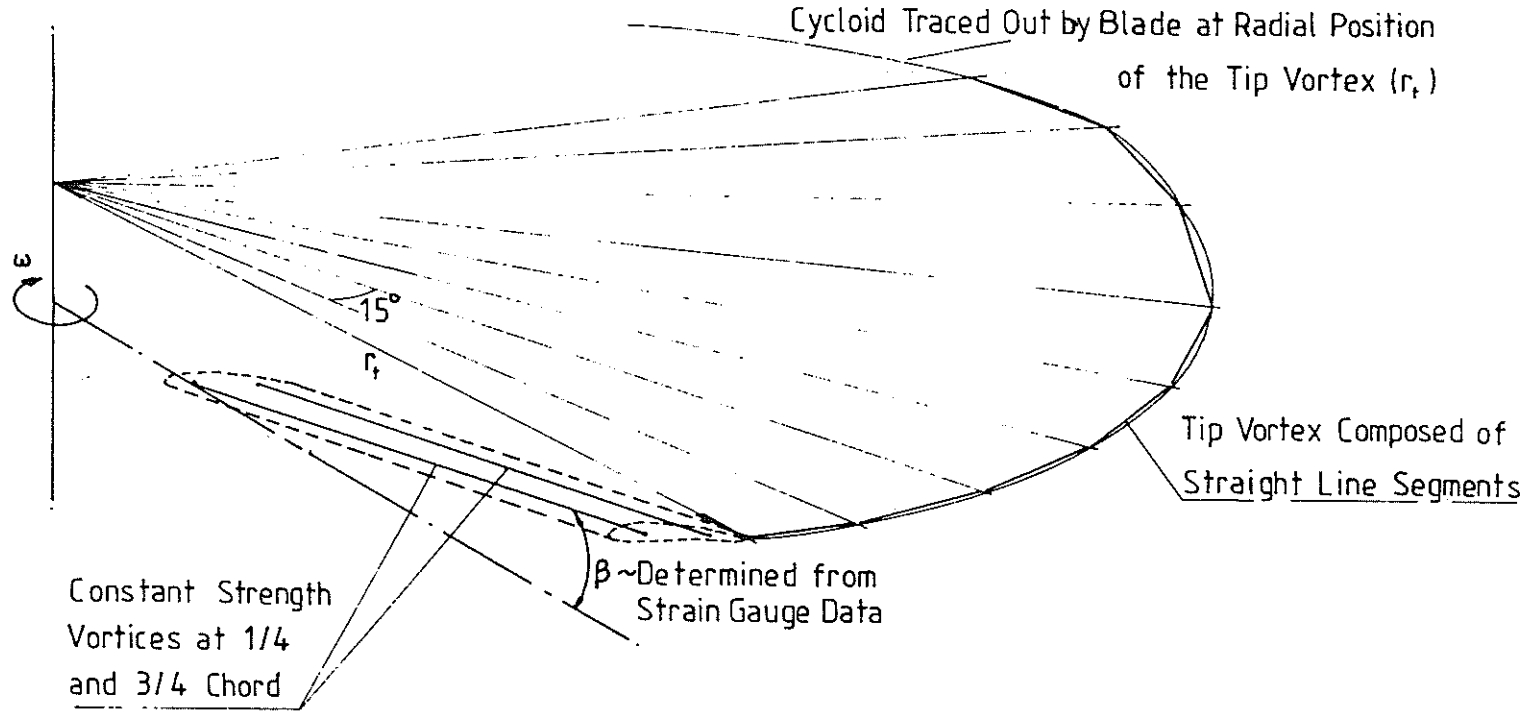

Figure 14
Schematic Showing Components Forming
the Curve Fitting Model.

Figure 15

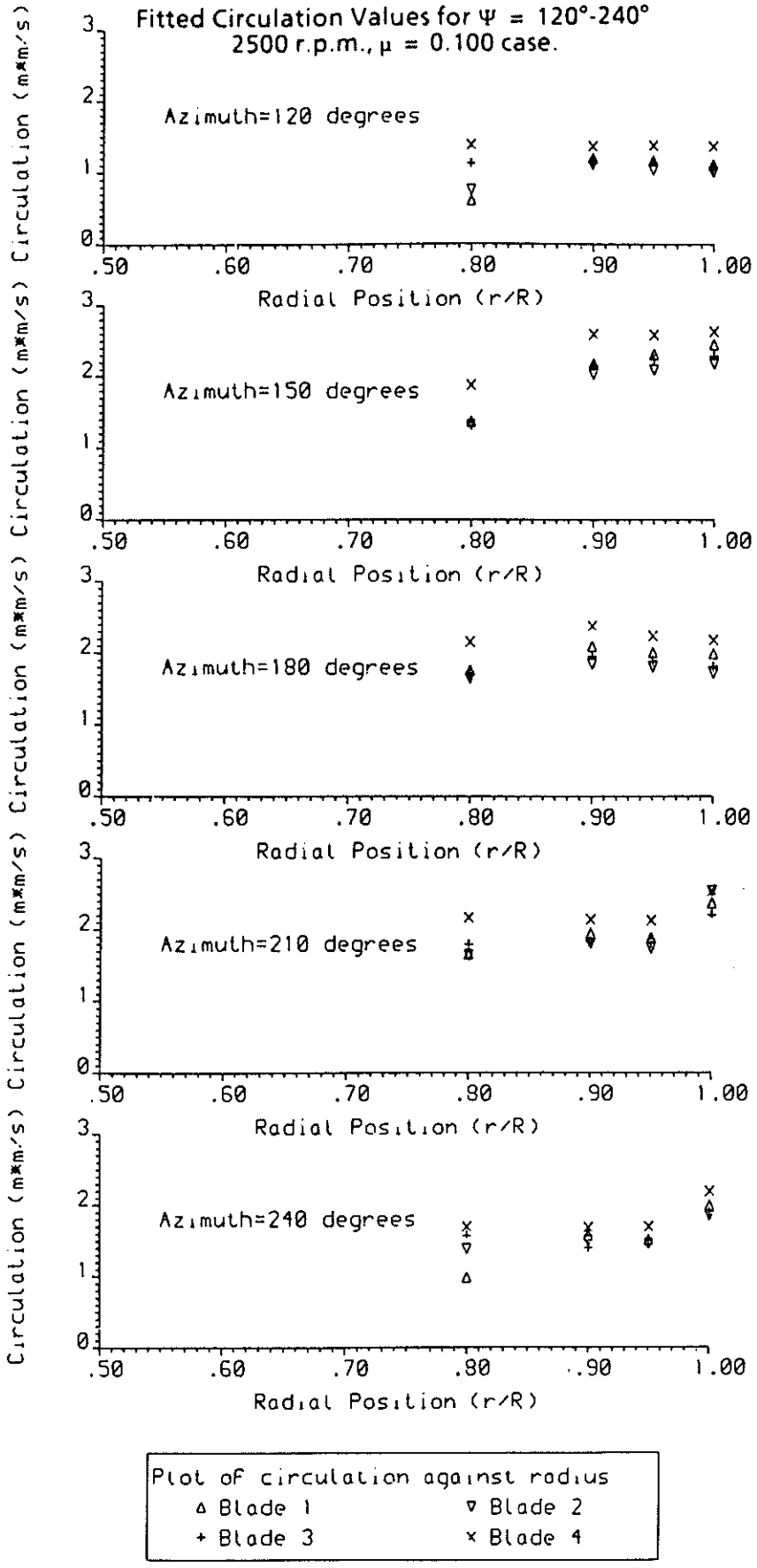
Fitted Circulation Values for Ψ = 120°-240°
2500 r.p.m., μ = 0.100 case.
Azimuth=120 degrees
Azimuth=150 degrees
Azimuth=180 degrees
Azimuth=210 degrees
Azimuth=240 degrees
Radial Position (r/R)
Circulation (m*m/s)
.50
.60
.70
.80
.90
1.00
0
1
2
3
Plot of circulation against radius
Δ Blade 1
▽ Blade 2
+ Blade 3
× Blade 4

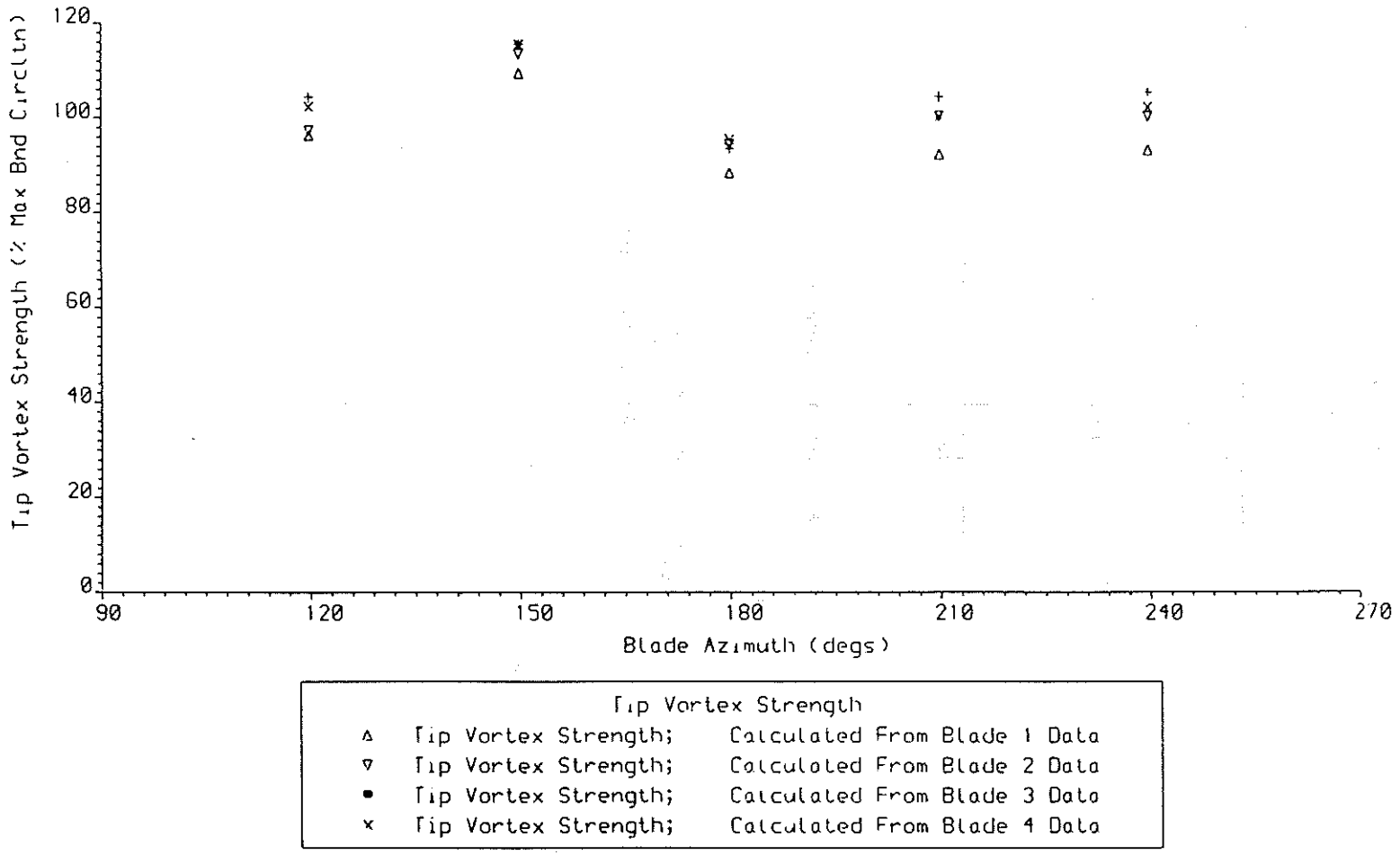

Figure 16
Fitted Tip Vortex Strength for Ψ = 120°-240°
2500 r.p.m., μ = 0.100 case.

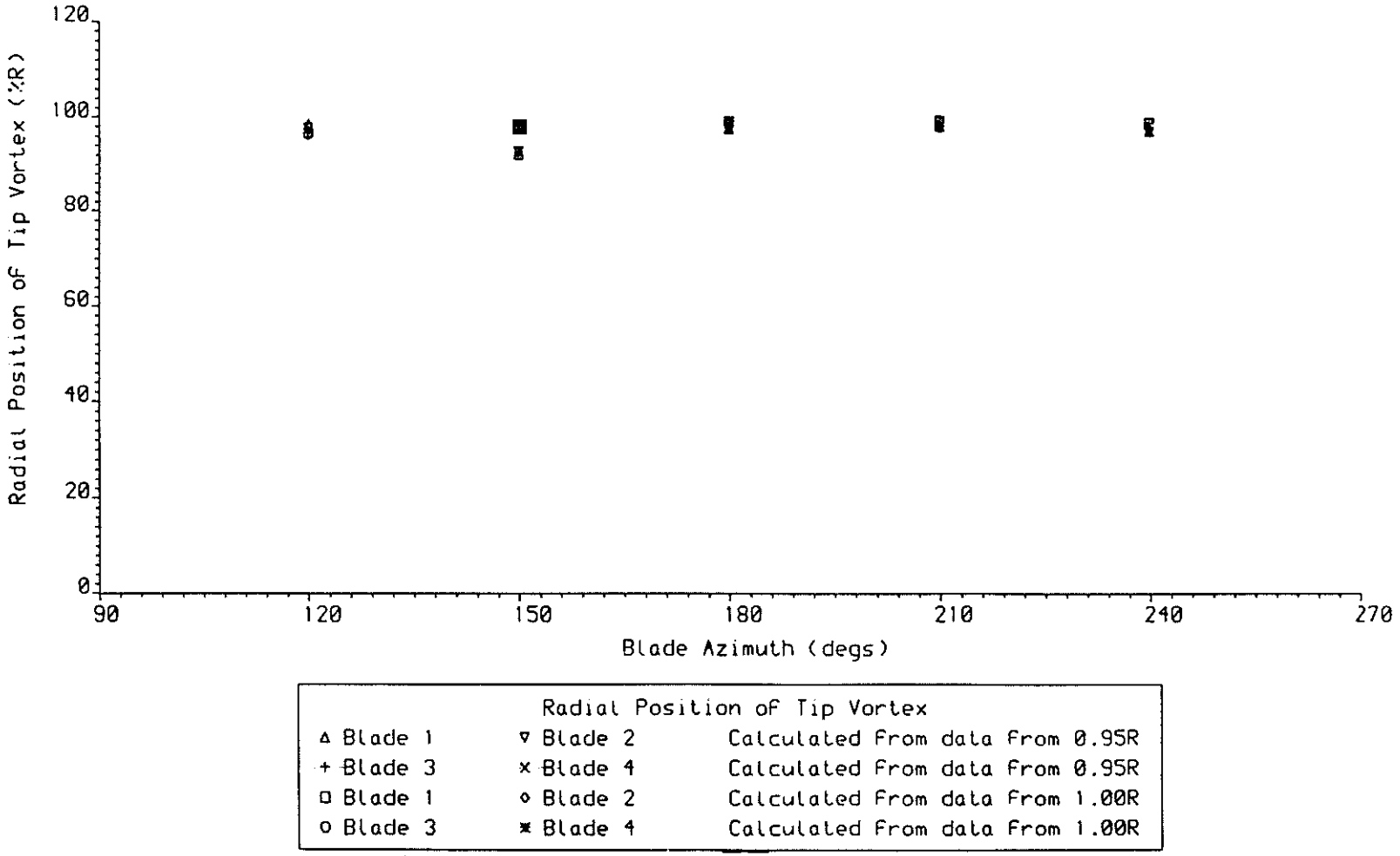

Figure 17

Fitted Tip Vortex Radial Position for Ψ = 120°-240°
2500 r.p.m., μ = 0.100 case.

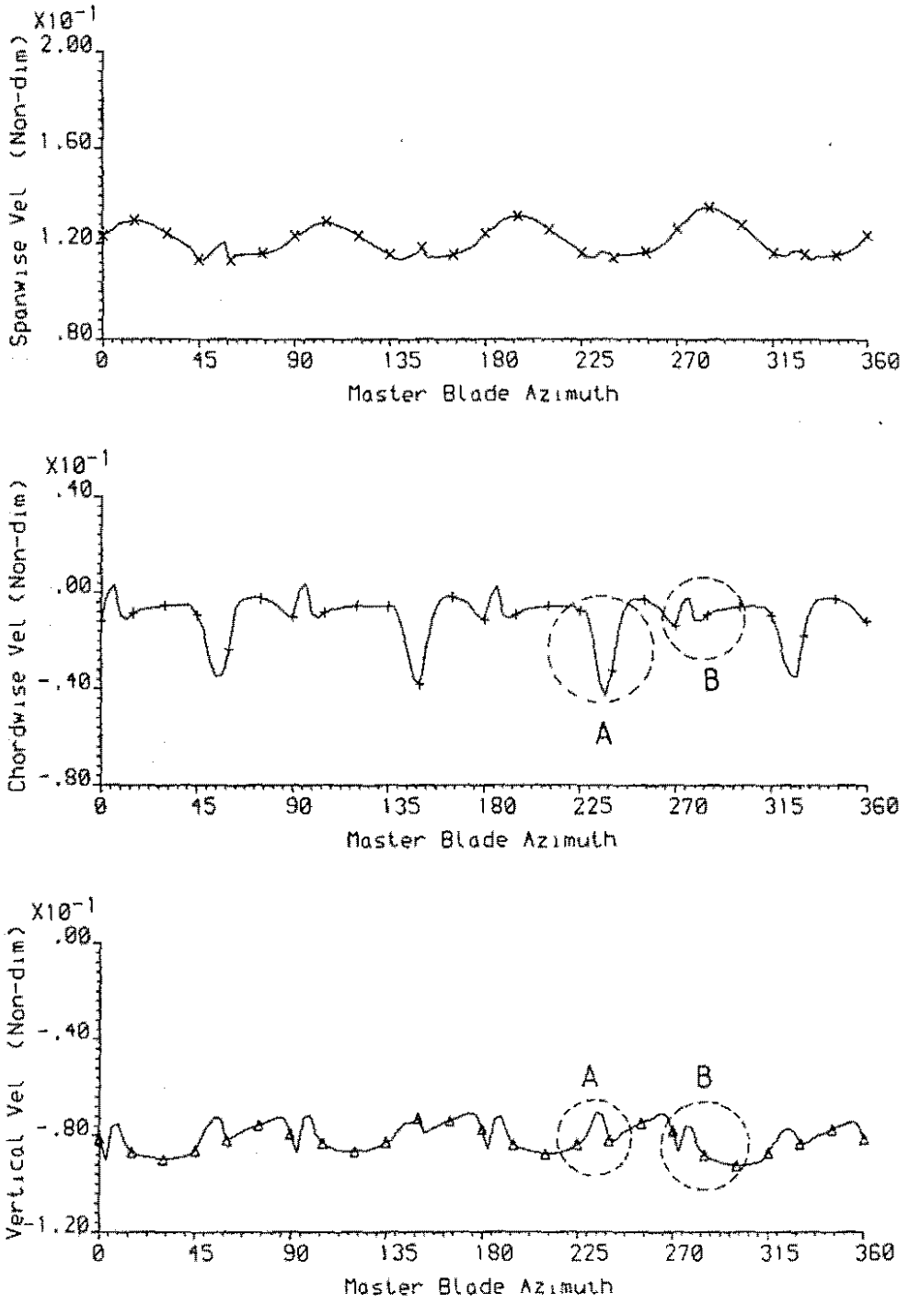
X10⁻¹
2.00
1.60
1.20
.80
Spanwise Vel (Non-dim)
0
45
90
135
180
225
270
315
360
Master Blade Azimuth
X10⁻¹
.40
.00
-.40
-.80
Chordwise Vel (Non-dim)
A
B
Master Blade Azimuth
X10⁻¹
.00
-.40
-.80
-1.20
Vertical Vel (Non-dim)
A
B
Master Blade Azimuth
Probe Azm= 0.0
Probe z/R=-0.075
Probe r/R= 0.950
Rotor RPM= 2500.0
Adv Ratio= 0.104
Revs Avgd= 32
× Spanwise
+ Chordwise
Δ Vertical
Symbols plotted at 15 degree intervals

Figure 18

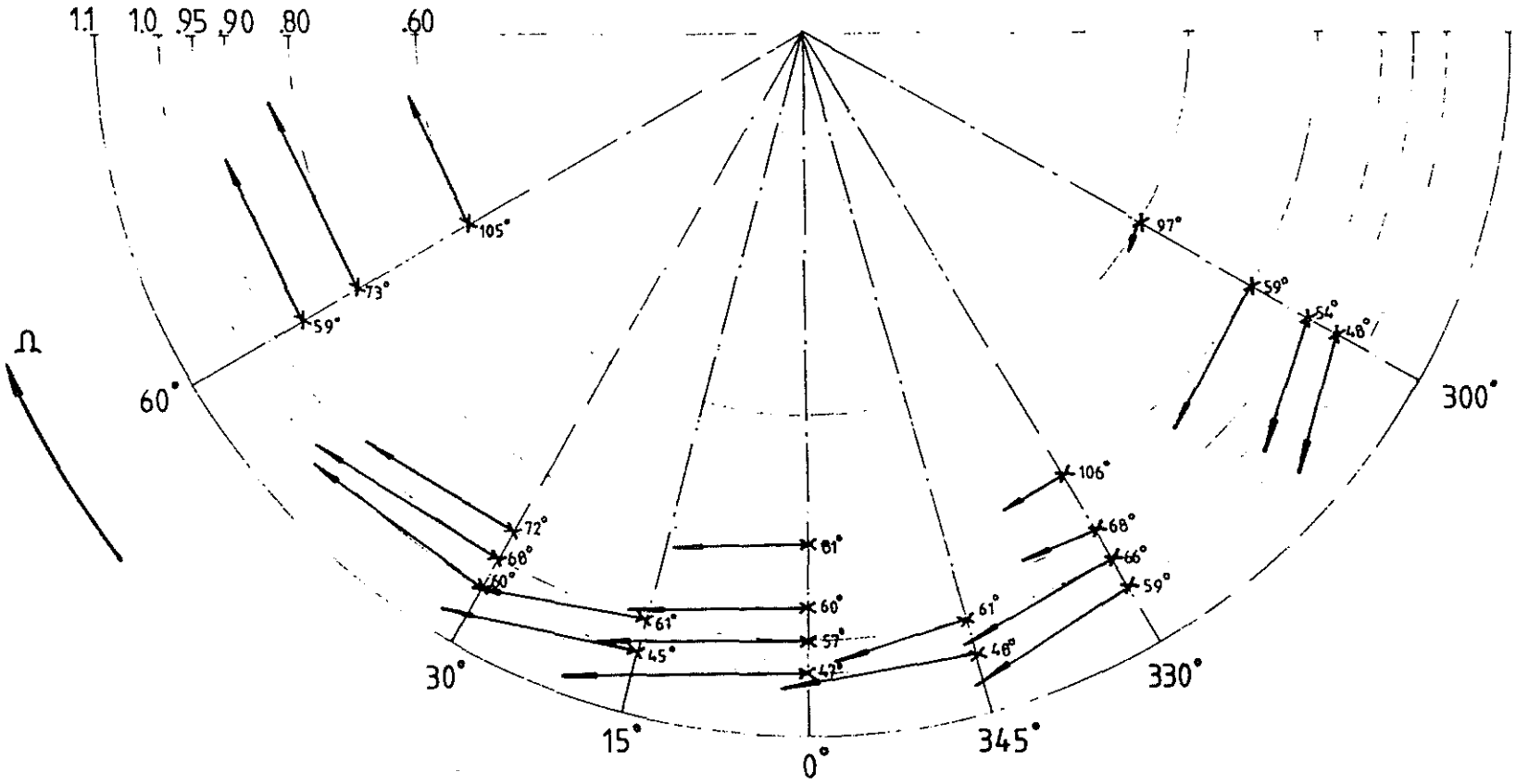

Figure 19

Plot Showing Direction and Magnitude of Velocity Increments Occuring in Peaks, 2500 r.p.m. μ = 0.100 case.

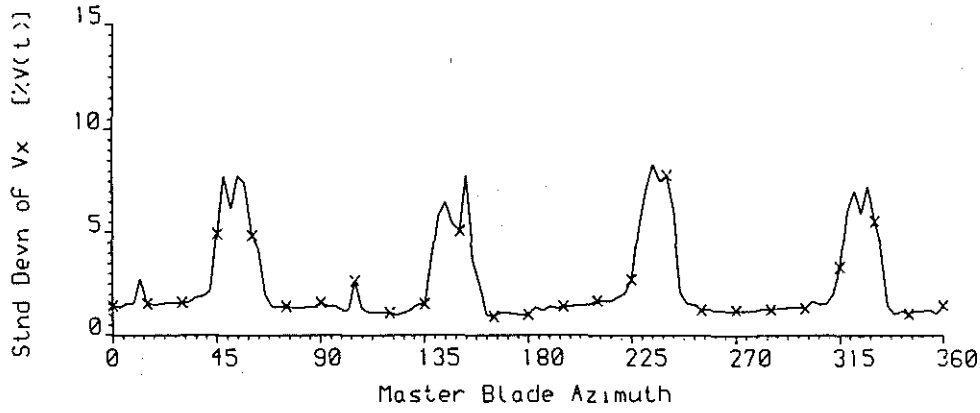

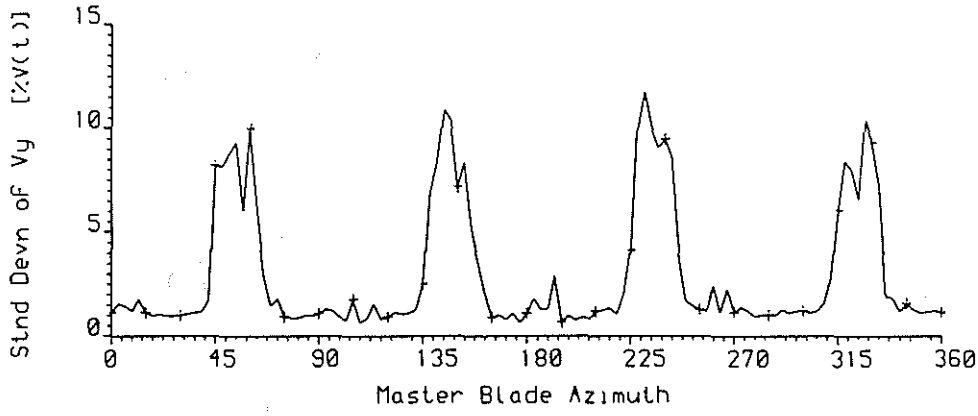

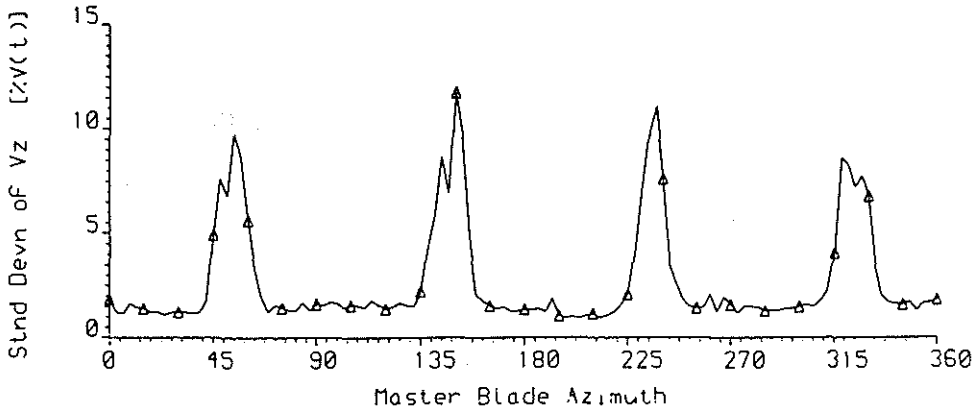

Probe Azm= 0.0	Rotor RPM= 2500.0	x X-compt
Probe z/R=-0.075	Adv Ratio= 0.104	+ Y-compt
Probe r/R= 0.950	Revs Avgd= 32	Δ Z-compt

Symbols plotted at 15 degree intervals

Figure 20

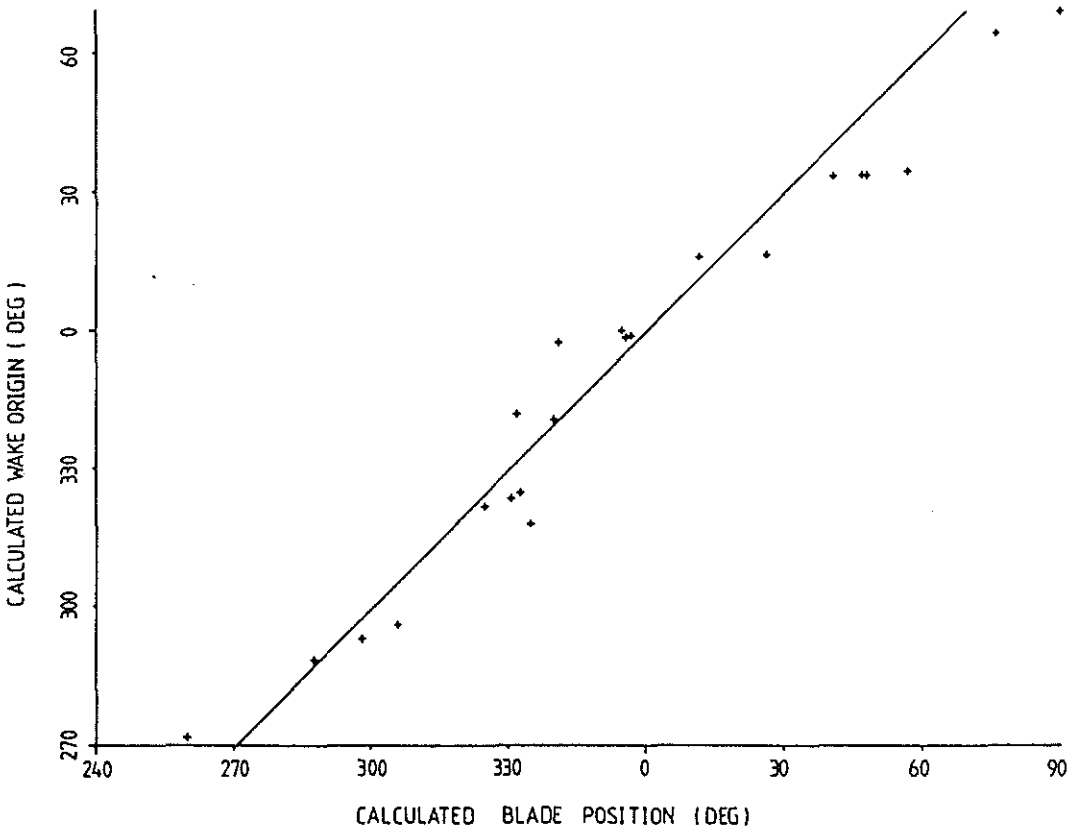

Figure 21
Plot Showing Calculated Blade Wake Origin
Against Calculated Blade Position.

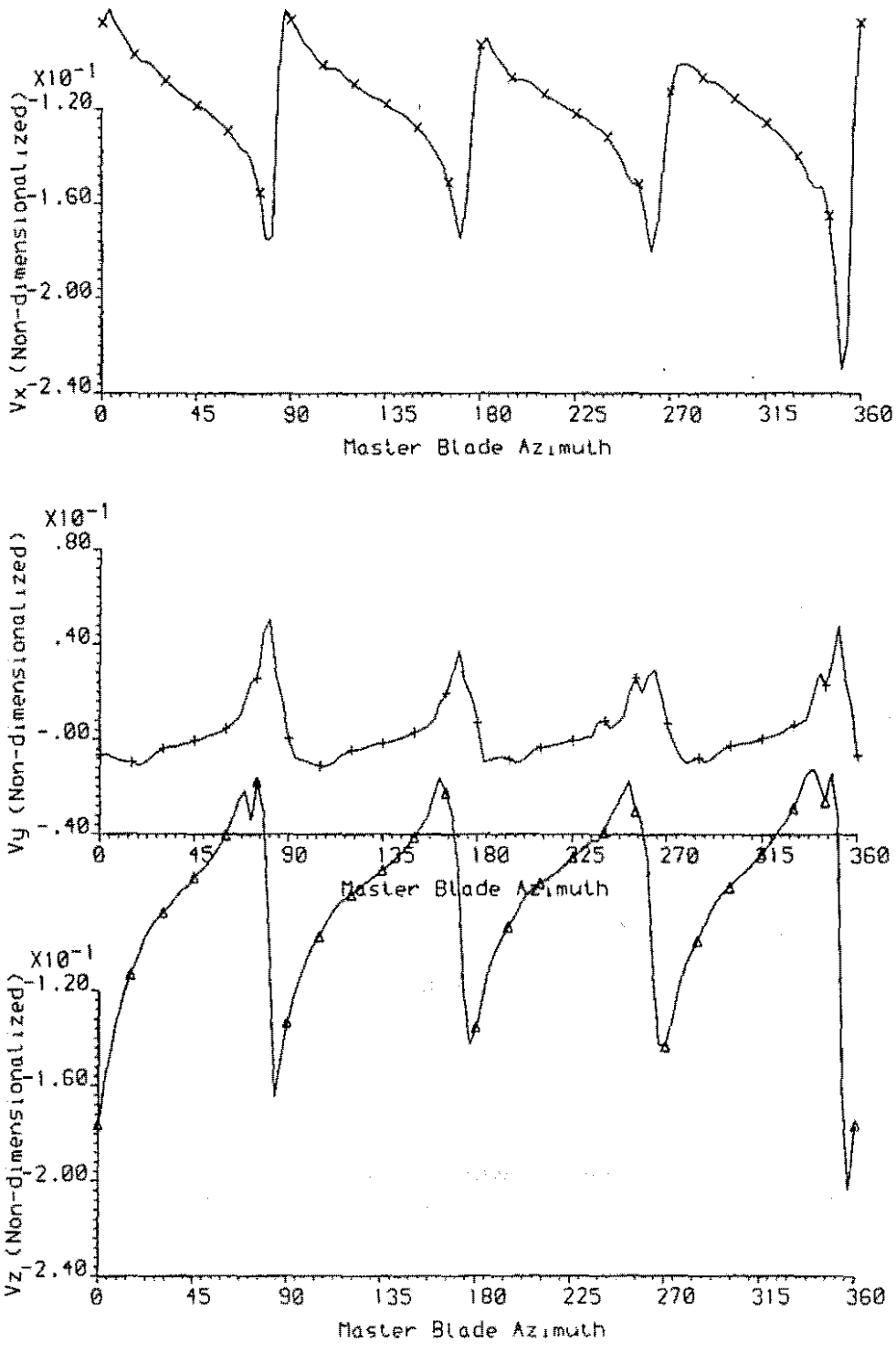
X10⁻¹
1.20
1.60
2.00
2.40
Vx (Non-dimensionalized)
0
45
90
135
180
225
270
315
360
Master Blade Azimuth
X10⁻¹
.80
.40
.00
-.40
Vy (Non-dimensionalized)
Master Blade Azimuth
X10⁻¹
1.20
1.60
2.00
2.40
Vz (Non-dimensionalized)
Master Blade Azimuth
Probe Azm= 15.0
Rotor RPM= 2470.4
x X-compt
Probe z/R=-0.075
Adv Ratio= 0.106
+ Y-compt
Probe r/R= 1.100
Revs Avgd= 8
Δ Z-compt
Symbols plotted at 15 degree intervals

Figure 22